Cell Reports

Article

Mechanisms of premotor-motor cortex interactions during movement initiation

Graphical abstract

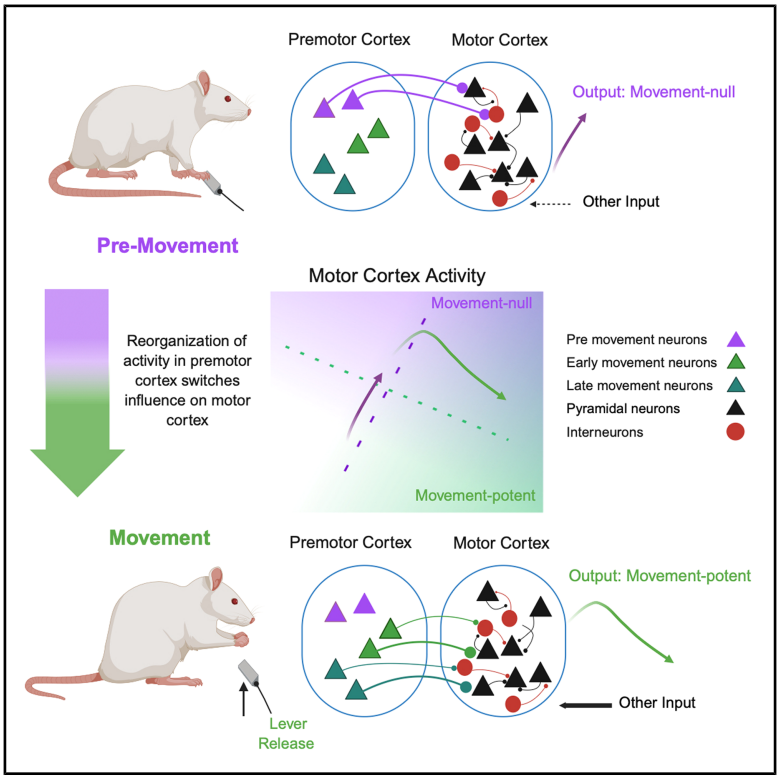

Highlights

- We propose a motor preparation model uniting inhibitory gating with the null space framework
- Silencing premotor to motor cortex projections, or either area alone, impairs behavior
- Premotor cortex subpopulations suppress and enhance motor cortical activity
- Premotor cortex targets excitatory and inhibitory neurons in motor cortex

Authors

Mansour Alyahyay, Julian J. Ammer, Gabriel Kalweit, ..., Andreas Vlachos, Joschka Boedecker, Ilka Diester

Correspondence

ilka.diester@biologie.uni-freiburg.de

In brief

Alyahyay, M. et al., investigate the interaction of rat premotor and motor cortex during the transition from preparation to movement. Combining electrophysiology, inverse reinforcement learning, optogenetics, and electron microscopy, this work reconciles elements of the movement-null hypothesis with circuit mechanisms from the inhibitory gating hypothesis during motor preparation.

Alyahyay et al., 2026, Cell Reports *45*, 117542
June 23, 2026
https://doi.org/10.1016/j.celrep.2026.117542

CellPress

Cell Reports

CellPress
OPEN ACCESS

Article

Mechanisms of premotor-motor cortex interactions during movement initiation

Mansour Alyahyay,[1,2,10] Julian J. Ammer,[1,2,10] Gabriel Kalweit,[2,3,4,10] Hao Zhu,[2,4,10] Ahmed Adzemovic,[1,2] Maria Kalweit,[2,3,4] Golan Karvat,[1,2] Artur Schneider,[1,2] Yixin Tong,[6] Mate D. Döbrössy,[6] Zoe Jäckel,[1,2] Cemal Akmese,[1,2,7] Andreas Vlachos,[2,5,8,9] Joschka Boedecker,[2,3,4] and Ilka Diester[1,2,5,11,12,*]

[1]Faculty of Biology, University of Freiburg, Freiburg, Germany
[2]IMBIT//BrainLinks-BrainTools Center, University of Freiburg, Freiburg, Germany
[3]Collaborative Research Institute Intelligent Oncology (CRIION), Freiburg, Germany
[4]Department of Computer Science, University of Freiburg, Freiburg, Germany
[5]Bernstein Center Freiburg, University of Freiburg, Freiburg, Germany
[6]Department of Stereotactic and Functional Neurosurgery, Medical Center, University of Freiburg, Freiburg, Germany
[7]Spemann Graduate School of Biology and Medicine (SGBM), University of Freiburg, Freiburg, Germany
[8]Center for Basics in NeuroModulation (NeuroModulBasics), Faculty of Medicine, University of Freiburg, Freiburg, Germany
[9]Institute of Anatomy and Cell Biology, Faculty of Medicine, University of Freiburg, Freiburg, Germany
[10]These authors contributed equally
[11]Senior author
[12]Lead contact
*Correspondence: ilka.diester@biologie.uni-freiburg.de
https://doi.org/10.1016/j.celrep.2026.117542

SUMMARY

Preparing and initiating movements at the right time is critical for goal-directed behavior. Before movement execution, motor cortical areas exhibit preparatory activity, which decreases from premotor to primary motor areas. During the shift from preparation to execution activity in neural state space transitions from movement-null to movement-potent dimensions. However, the circuit-level mechanisms underlying this shift remain unresolved. Here, we demonstrate that projections from the rat premotor cortex (rostral forelimb area [RFA]) to the primary motor cortex (caudal forelimb area [CFA]) encode primarily pre-movement activity. Optogenetic inhibition of these projections has behavioral effects comparable to inhibiting either RFA or CFA alone. During preparation, RFA projections enhance and suppress CFA neurons similarly, affecting activity along CFA's preparatory dimension. During movement, RFA's influence shifts predominantly to excitatory, aligning with CFA's movement-potent dimension. These results establish a mechanistic link between neural state space concepts and underlying circuit mechanisms, providing an intuitive model for movement control.

INTRODUCTION

Motor cortex activity has been classically linked to movements.[1,2] However, motor cortical neurons can become active long before volitional movements are initiated.[3,4] This activity is thought to represent the internal preparation of movement, which brings the involved neuronal networks into a state that facilitates selective movement execution.

In primates, premotor areas primarily contribute to movement preparation,[5–9] while the primary motor cortex is engaged in movement execution.[3,8,10,11] In line with this view, neurons in the premotor cortex show more preparatory activity. Given the direct input from the premotor cortex to the primary motor cortex, an outstanding question remains: why does preparatory activity in the premotor cortex not immediately activate the primary motor cortex and trigger movement? Two primary hypotheses have been proposed to answer this question. (1) The gating hypothesis suggests that during movement preparation, the premotor cortex activates both inhibitory and excitatory neurons in the primary motor cortex equally. Upon movement initiation, inhibition is lifted, allowing excitatory neurons to pass signals downstream.[12,13] This hypothesis, while appealing in its simplicity and intuitive nature, has not been substantiated by cortical neural data.[13–15] (2) The null space hypothesis explains neural activity through a dynamical systems framework and posits that preparatory activity occurs in an output-null dimension, where neural population activity cancels out at the downstream target, so that preparatory activity in the premotor cortex does not reach the motor cortex and does not cause premature movement.[16–18] In this framework, output-null refers to the communication between two areas and movement-null refers to neural activity in the absence of movement. Under this definition, preparatory activity in premotor cortex is movement-null, but if the preparatory activity propagates to and modulates activity in the primary motor cortex, it is output-potent relative to the motor cortex, even if it does not yet directly drive movement. However, the circuit mechanisms underlying these population dynamics and, in particular, the role of premotor to primary

motor cortex connections in mediating the switch from movement-null to movement-potent activity in motor cortex remain elusive.

In rodents, the rostral and caudal forelimb areas (RFA and CFA) are distinct cortical regions[19] likely corresponding to premotor and primary motor areas for forelimb control.[20–23] RFA neurons exhibit weaker preference to contralateral movements than CFA neurons,[24] a feature used to distinguish primary motor areas from premotor areas in primates. How these areas interact during movement planning and execution remains unclear. Both areas contain neurons projecting to the cervical spinal cord and subcortical regions,[22,25,26] and intracortical microstimulation of RFA and CFA elicits specific forelimb movements.[27,28] In addition, neuronal activity in RFA and CFA is remarkably similar across a range of tasks,[29–31] suggesting joint control of movement execution.[32] However, the reciprocal connectivity between RFA and CFA is asymmetric, suggesting a hierarchical organization with RFA more akin to a premotor area.[22,33–35] In line with this view, activity in RFA has been shown to lead CFA activation[36,37] in learned motor tasks and is thought to integrate higher-order contextual information.[31,38,39] To investigate how the rat RFA influences CFA during the distinct phases of motor preparation and movement execution, we employed electrophysiology, pathway-specific optogenetics, photo-tagging, electron microscopy, and inverse reinforcement learning in freely moving rats performing prepared movements.

We observed a substantial reconfiguration of activity and interareal communication from pre-movement to movement phase, leading us to propose the switching population hypothesis: this hypothesis integrates aspects of the gating and null space hypotheses, assigning specific neuronal elements to neural state space dynamics. Our findings demonstrate that RFA transmits information via direct projections to parvalbumin (PV)-positive interneurons and excitatory neurons in the CFA. During pre-movement, RFA exerts balanced excitatory and inhibitory effects on CFA neurons. However, upon movement initiation, RFA's influence shifts predominantly toward excitation. Additionally, the subset of CFA neurons that are affected by RFA changes between these phases. Collectively, these changes transition RFA's influence from driving activity along the movement-null direction during preparation to acting along the movement-potent direction during execution.

RESULTS

Movement execution time is decoded equally well from RFA and CFA activity

To investigate the role of RFA and CFA in movement planning and execution, we trained freely moving rats to conduct prepared movements.[40,41] Rats initiated trials by moving a lever with their preferred hand and had to wait while holding the lever until a vibrotactile stimulus (0.3 s) was delivered via the lever, which served as the go cue (Figure 1A). In response to the go cue, the rats had to release the lever within a response window of 0.6 s to receive a liquid reward. To discourage timing, rats were pseudo-randomly required to hold the lever for 0.6 or 1.6 s (short or long delay). Although the rats learned to wait for and respond to the cue, they also made errors by either releasing the lever too early or too late (i.e., outside the allowed response window), thus not implementing the optimal strategy (premature trials: 52.24% ± 4.42%, correct trials: 44.29% ±4.84%, delayed trials = 3.46% ± 1.08%; Figure 1B). The increased error rate might be related to the light force that the rats had to sustain during the delay period, which represents a deviation from previous movement preparation tasks (see section "limitations of the study"). To reveal the individual strategies of the rats, we leveraged a concept from reinforcement learning to present the internal task model of the rats as a series of states in a Markov decision process ([MDP], Figure 1C).[42,43] Intuitively, this MDP models the task as a sequence of decision steps in 0.2-s bins (states): at each step, the animal decides whether to hold or release the lever (actions), which results in either success or error as an outcome. This formalization of the task allowed us to apply a machine learning algorithm based on inverse reinforcement learning (NeuRL) to extract the intrinsic reward, which was associated with each transition between the states (Figure S1A).[44] Note that here the "intrinsic reward" refers to the reward considered in the NeuRL model (in particular, the MDP), not the liquid reward of the rat. This internal model, which can be learned for each individual animal, can then be used to decode behavior from neural data (where it outperformed classical neural network classifiers[42]) as well as for making predictions about the functional role of different neuronal populations, which we will use later on in the article. Equipped with the individual task models of each rat (Figure 1D), we asked if more task-relevant information is encoded in RFA or CFA, or alternatively, if these regions are equally informative. To obtain the required neuronal data, we implanted 32-electrode silicon probes in RFA or CFA and recorded neuronal activity across cortical layers (N = 10 rats split into two groups of N = 5 per forelimb area; Figure 1E; Table S1). We then decoded the animal's action selection policy by calculating the probability of whether a release or hold was performed by the animal, from their neural activities for each time step of the MDP. To quantify decoding accuracy, we calculated the log likelihood as the log of the product of the action likelihood (i.e., the probability of observing the animal's true behavior based on our prediction) for all time steps along the trial. The decoding of lever release times did not significantly differ between the recordings from CFA or RFA, as indicated by the small decoding error, quantified as negative log likelihood, for both areas (RFA: mean = 0.56; confidence interval [CI], [0.51, 0.62]; CFA: mean = 0.65; CI, [0.58, 0.71]; p = 0.13; t test, 1 session selected per animal to match neuron numbers across regions, nRFA = 102 neurons in N = 5 rats; nCFA = 107 neurons in N = 5 rats, Figure 1F, all sessions; Figure S1B). The decoding of task initiation time was associated with a generally greater model error in a similar manner for both areas (Figure S1C, initiation vs. release for RFA, p = 0.017, paired t test, N = 5; for CFA, p = 0.45, paired t test, N = 5 rats). These results suggest that both areas carry similar degrees of task-relevant information.

RFA and CFA jointly contribute to movement execution, with RFA being primarily active before movement and CFA during movement

Since we successfully decoded the release time equally well from both RFA and CFA, we next investigated whether this indicates

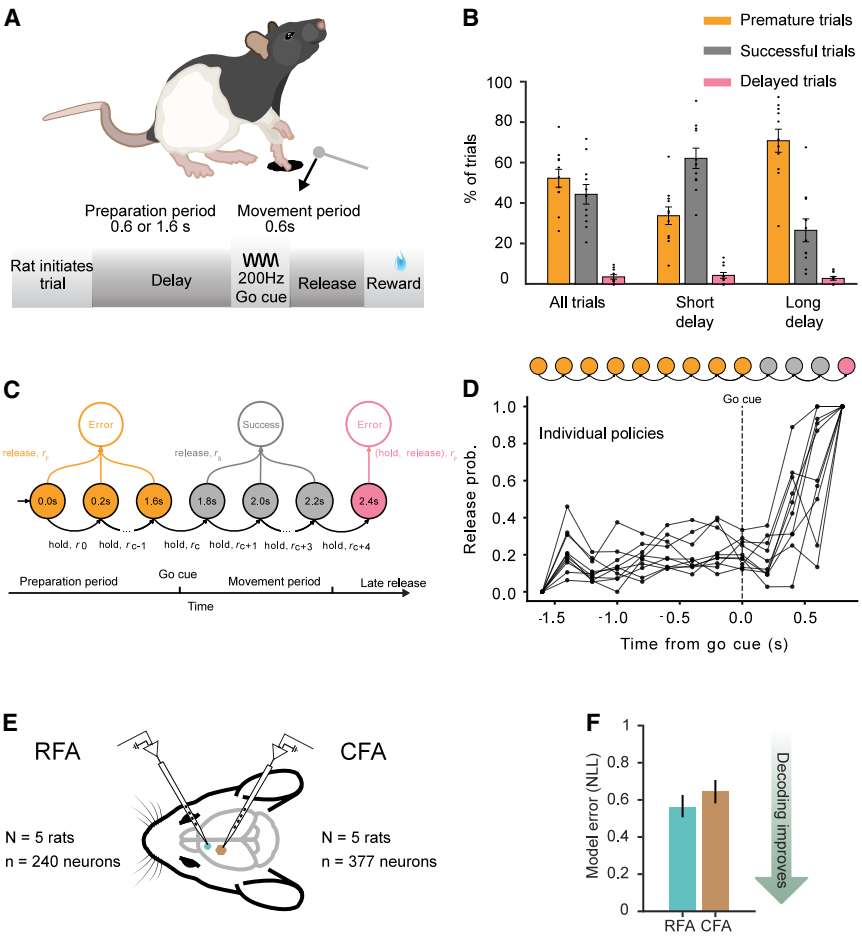

Figure 1. Individually inferred task models support equal decoding of performance from RFA and CFA

(A) Simplified illustration of the task. To initiate a trial, the freely moving rat had to move a lever horizontally and hold it. After a pre-movement period of 0.6 or 1.6 s, the lever vibrated, which was the go cue. In response to the go cue, the rat had to release the lever within a response window of 0.6 s to receive a reward; otherwise, the trial was considered a delayed trial. Releases during the preparation period were considered premature releases. Correct trials were signaled with a click tone, while both premature and delayed trials were followed by a 1-s timeout and white noise.

(B) Behavioral performance in the first recording session of each animal ($N = 11$ rats); correct responses in all trials: 44.2%, correct responses in trials with short delay: 62.8%, correct responses in trials with long delay: 26.5%).

(C) The internal model of the rat is formulated as a series of states of an MDP based on the possible actions and states. Based on inverse reinforcement, learning the rats' strategy was estimated and a reward value was extracted.

(D) Release probabilities in each time bin during the trials as predicted based on the individual rat policies.

(E) Schematics of extracellular recordings of neuronal activity in RFA or CFA ($N = 5$ rats for each area, one session per rat with similar number of neurons across rats).

(F) Model error for decoding the release time via NeuRL quantified as negative log likelihood (NLL). Release time is decoded similarly well from RFA or CFA (RFA: mean = 0.56; CI, [0.51, 0.62]; $N = 5$ rats; CFA: mean = 0.65; CI, [0.58, 0.71]; $N = 5$ rats; $p = 0.13$; t test).

See also Figure S1.

that the task-related responses of individual neurons are similar in these two forelimb areas. Indeed, we found that neurons of both areas showed task-related activity to a similar degree when aligned to movement onset, with 60% of neurons in RFA (n = 144/240 in $N = 5$ rats) and 54% in CFA (n = 205/377 in $N = 5$ rats, Figures 2A–2E) exhibiting significant modulation between the pre-movement and the movement period ($p < 0.05$; t test).

We further objectively separated the modulated neurons based on their averaged Z-scored firing rates in the pre-movement and movement phases using k-means clustering. To compare response clusters of the two regions directly, we pooled all neurons from both areas for the clustering. Despite the neuronal heterogeneity in response profiles, the clustering led to three clusters with distinct response types: one cluster with prominent pre-movement activity and two clusters with early or late movement related activity, respectively (Figures 2B–2D and 2F–2H; Figures S2A and S2B).

In line with the role of RFA in motor preparation, we found the dominant subgroup in RFA to be the pre-movement cluster at 72%. In contrast, and highlighting the role of the CFA in

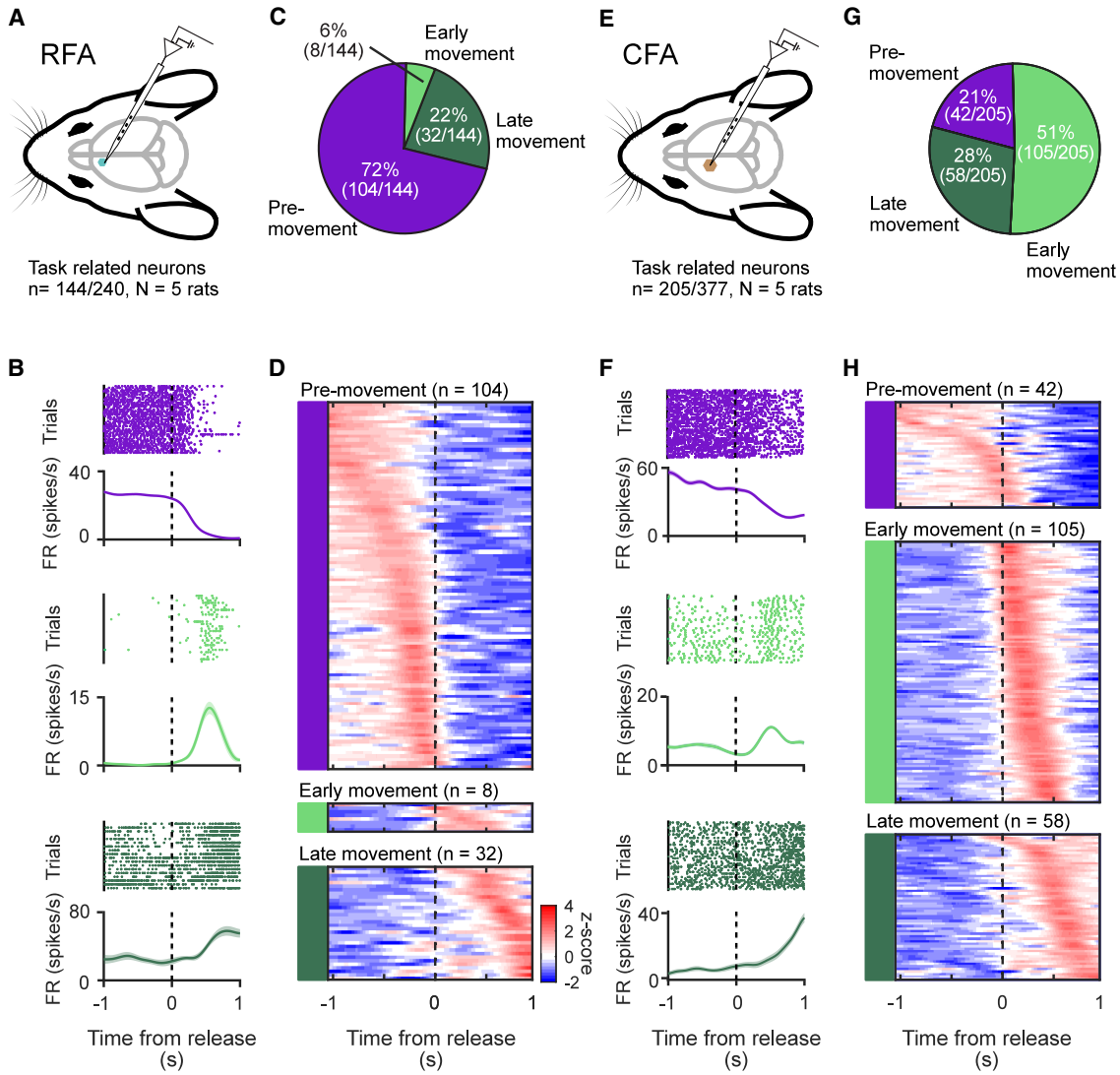

Figure 2. RFA is primarily active in the pre-movement period, while CFA shows greater activity during movement

(A) Schematics of extracellular recordings in RFA (*N* = 5 rats, modulated units *n* = 144/240 neurons).

(B) Neuronal example response types for individual *k*-means clusters in RFA. Purple, pre-movement example; light green, early movement example; darker green, late movement example. (Top) Raster plots of individual trials, (bottom) firing rate average across trials.

(C) Proportions of RFA-modulated neurons grouped according to their clustering.

(D) Normalized average firing rates (*Z* score) of all modulated neurons in RFA.

(E–H) Same as (A–D), but in CFA (*N* = 5 rats, modulated units *n* = 205/377).

See also Figure S2.

movement execution, 79% of the CFA neurons were classified into either the early (51%) or late (28%) movement clusters, clearly distinguishing it from RFA where only 28% of the neurons were part of the two movement clusters.

These findings support the characterization of RFA as a premotor cortex, exhibiting more pronounced preparatory activity, and CFA as a primary motor cortex, with activity primarily, although not exclusively, focused on movement execution.

Based on the prominent pre-movement activity of the RFA, we hypothesized that inhibiting RFA optogenetically during the pre-movement period would have a greater effect than inhibiting CFA during the same period. To selectively suppress neuronal activity in these regions individually, we expressed the inhibitory opsin eNpHR (AAV5-hSyn-eNpHR-EYFP) (Figure S2C). Both RFA and CFA suppression for 0.5 s during the pre-movement period reduced releases during the laser stimulation without interfering with the ability to hold the lever (Figures S2D–S2F). These results suggest that both RFA and CFA facilitate movement initiation. However, the premature error rate was reduced more robustly when RFA was inhibited (Figure S2F, RFA: premature error rate median = −0.11 CI [−0.18, −0.06]; CFA: premature error rate median = −0.05 CI [−0.13, 0.01]).

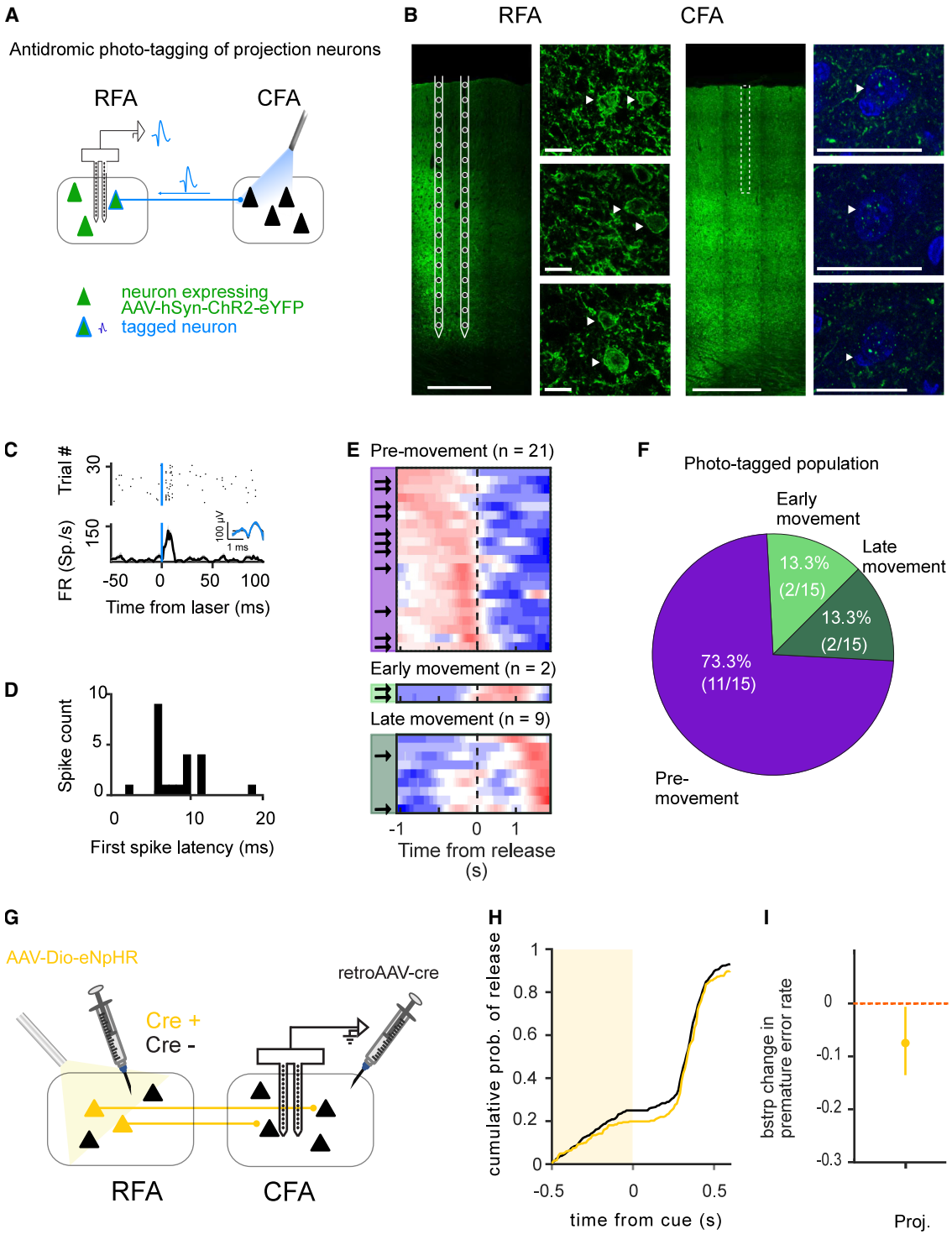

Figure 3. Neurons projecting from RFA to CFA encode primarily pre-movement activity

(A) Schematic of the photo-tagging experiment. AAV5-hSyn-ChR2-eYFP was injected into the RFA ($N = 3$). A silicon probe was implanted in RFA, and an optical fiber was placed in the CFA. At the end of the behavioral session, 1-ms light pulses were delivered to the CFA via the optical fiber to induce antidromic spikes by activating ChR2 in RFA axonal terminals in CFA (blue waveforms).

(B) (Left) Coronal section through the RFA with cells expressing AAV5-hSyn-ChR2-eYFP including estimated electrode positions in RFA; white outlines, electrode shafts in RFA; scale bar, 500 µm (left). Examples of RFA neurons expressing AAV5-hSyn-ChR2-eYFP; scale bars, 20 µm; white arrows point to labelled somata in

(legend continued on next page)

Neurons projecting from RFA to CFA encode primarily pre-movement activity

Given the converging electrophysiological and optogenetic evidence regarding the pre-movement role of RFA neurons, we asked whether and how this information is conveyed to CFA. To identify RFA neurons projecting to the CFA, we triggered back-propagating (antidromic) spikes in the RFA by stimulating its axons within the CFA (Figure 3A). We injected AAV5-hSyn-ChR2-eYFP into the RFA, implanted a silicon probe in RFA, and inserted an optical fiber into the CFA (Figures 3A and 3B; $N = 3$ rats; Table S2). In total, 21 of 45 neurons (47%) recorded in RFA were "photo-tagged," as indicated by short latency spike responses to photostimulation in CFA, marking them as putatively projecting from RFA to CFA (Figures 3C and 3D). In a subset of photo-tagged neurons, we were able to conduct collision tests due to spontaneously occurring spikes just prior to photostimulation. These spontaneously occurring spikes were associated with subsequent spike failures during photostimulation, likely caused by collisions of spontaneously occurring and photo-triggered spikes in the axon. Variability and latency of the photo-evoked spikes of all putatively photo-tagged neurons fell into the same range as for the collision-tested neurons (Figures S3A and S3B), making them likely candidates for direct projection neurons. Fifteen tagged neurons were significantly modulated during the task ($p < 0.05$, t test). In line with the response profiles in the RFA, the majority of these tagged neurons were part of the pre-movement cluster (73%, Figures 3E and 3F). To test the behavioral role of the RFA to CFA projecting neurons, we optogenetically silenced these neurons during the pre-movement phase (Figure 3G). Strikingly, manipulating this subpopulation had a similar effect as targeting all neurons in RFA or CFA (Figure S3C) and reduced premature releases during the pre-movement phase (premature error rate median −0.07 CI, [−0.14, −0.01]; Figures 3H and 3I). Most likely this behavioral effect is due to inhibiting the transition from pre-movement to movement activity that would normally occur during the hold phase (i.e., prior to the cue) in premature trials. In line with this view, inhibiting the projecting neurons during the movement phase also slightly delayed movement (Figure S3D)

As we cannot manipulate the individual subpopulations with the current experimental setup to support this interpretation, we leveraged NeuRL to make predictions about the behavioral roles of the pre-movement and movement clusters (see STAR Methods and Figure S3E for simulation of control conditions). To support the feasibility of this approach, we first compared experimental and simulation data by simulating the inhibition of all RFA to CFA projecting neurons in our photo-tagging dataset. In line with the optogenetic experiments, simulated inhibition of projecting neurons during the pre-movement period reduced early releases (Figures S3F and S3G). We next asked how the main subgroups within the neurons projecting from RFA to CFA, i.e., the pre-movement and the movement neurons, might affect behavior individually (Figure S3H). Interestingly, NeuRL predicted that pre-movement and movement subpopulations had opposing effects on behavior. Inhibiting the pre-movement subpopulation during the pre-movement phase shifted the release time leftward, resulting in more premature errors, while inhibiting the movement neurons delayed releases, thereby reducing premature errors. Together, these predictions suggest that the projecting neurons contain two competing subpopulations affecting behavior in opposite ways. The pre-movement neurons could, therefore, play a role in withholding the movement during the preparation phase. Alternatively, they might be needed to actively hold down the lever during the preparation phase, although we were not able to reliably decode the lever position from RFA activity during the hold phase (linear regression model, $R^2 = 0.25 \pm 0.03$ SEM for RFA), making this alternative interpretation less likely.

RFA targets excitatory and inhibitory circuits in CFA

According to the null space hypothesis, preparatory activity should cancel out in the target region and result in no net activity changes. How could this happen given that increased pre-movement activity is dominant in the projections from the RFA to the CFA? One potential solution could be a sign inversion of part of the input signal via inhibitory interneurons in CFA. To examine this option, we asked if the RFA indeed targets inhibitory interneurons in CFA.

To address this question, we used transmission electron microscopy to investigate RFA synapses targeting CFA neurons. We employed pre-embedding immunogold labeling of EYFP to identify EYFP-labeled RFA axonal terminals in CFA (Figures 4A and 4B). According to the functional Gray synapse concept, we classified synapses as asymmetric (excitatory, Figure S4A) or symmetric (inhibitory, Figure S4B).[45] The vast majority of the synapses were asymmetric, suggesting these synapses originate from excitatory neurons (asymmetric synapses: $n = 97/100$, symmetric synapses: $n = 3/100$, Figure S4C).

To test for connections onto inhibitory interneurons, we stained coronal CFA sections with anti-PV antibodies and

RFA (right). (Right) Coronal section of the CFA with RFA axons expressing eYFP in CFA; dashed white rectangle, optical fiber position in CFA; scale bar, 500 μm (left). Examples of CFA neurons labeled with DAPI (blue) close to RFA axons (green); scale bars, 5 μm; white arrows point to labelled axons in CFA (right).
(C) Raster and average firing rate of a tagged neuron. (Inset) mean waveform of simultaneous spikes (black) and antidromically induced spikes (light blue).
(D) Latency of the first spike after the light pulse of the example tagged neuron in (C).
(E) Normalized average firing rates (Z score) of all neurons. Black arrows, photo-tagged neurons.
(F) Proportions of different subpopulations in the photo-tagged population.
(G) Schematic for inhibition of neurons projecting from RFA to CFA. AAV-Dio-eNpHR-eYFP was injected bilaterally into the RFA, and a retrograde viral vector carrying cre recombinase (retroAAV-cre) was injected into the CFA. Optical fibers were implanted bilaterally into the RFA.
(H) Cumulative probability of release times in control (black) and after inhibition (yellow) during the pre-movement period relative to cue onset ($N = 4$ rats with $n = 32$ sessions).
(I) Median bootstrapped change in premature error rate with 95% confidence interval for inhibition of the RFA to CFA projecting neurons; dashed line indicates 0 change, $n = 1{,}000$ bootstraps with mean of $n = 15$ sessions each.
See also Figure S3.

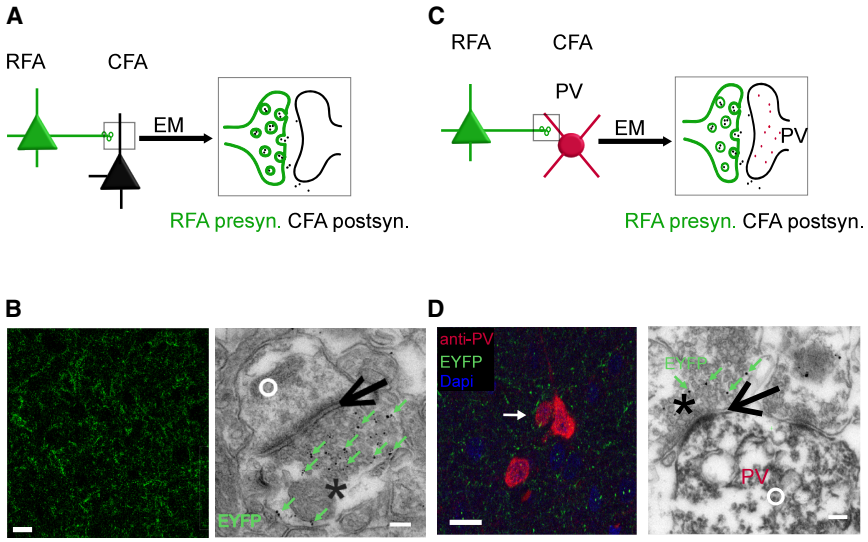

Figure 4. RFA targets excitatory as well as inhibitory neurons in CFA

(A) Simplified schematics for structurally investigating RFA input to CFA. We injected AAV-hSyn-eNpHR-eYFP in RFA ($N = 4$) to detect synaptic terminals of RFA inputs to CFA in electron microscopy.

(B) (Left) Confocal image of coronal section through the CFA with AAV-hSyn-eNpHR-eYFP expressing EYFP in RFA axons. (Right) Electron microscopy (EM) image in the CFA showing an RFA axonal terminal contacting a dendritic spine in CFA.

(C) Schematics for investigating RFA input to PV interneurons in CFA. RFA input was labeled with EYFP; parvalbumin (PV)-positive interneurons were labeled with a PV antibody.

(D) (Left) Example of a PV interneuron in the CFA targeted by axons from RFA. Confocal image of a coronal section through the CFA expressing EYFP in RFA axons projecting to CFA. Confocal image example of coronal section (left). EM image in the CFA showing an RFA axonal terminal contacting a spine of a PV interneuron in the CFA (right).

Scale bar in confocal images, 20 μm; scale bar in EM images, 100 nm; white arrow, PV interneurons; green arrows in EM, immunogold staining against EYFP particles in RFA pre-synaptic terminal; black asterisk, pre-synapse; black arrow, synaptic cleft; white circle, postsynapse.

See also Figure S4.

searched for EYFP-labeled axons across layers. We found labeled axons that formed synapses onto PV interneuron dendrites in 3 of 4 rats (Figures 4C and 4D) as well as a majority of contacts on non-PV-stained structures. These results demonstrate that RFA affects the CFA local circuit by targeting both excitatory neurons and PV interneurons.

RFA influence on CFA is balanced during pre-movement and excitatory during movement

Given that RFA targets both excitatory and inhibitory neurons in CFA, we asked if and how the RFA influence on CFA would "switch" from inhibition to excitation between preparation to movement. We recorded CFA neurons while simultaneously inhibiting RFA in a subset of trials in either pre-movement or movement period (Figure 5A). We limited the inhibition of the RFA to CFA projecting neurons by injecting rAAV2-retro CAG-Cre in CFA and a cre-dependent eNpHR in RFA (Figure 5B; Table S3). The number of CFA neurons modulated by inhibiting RFA neurons projecting to CFA remained consistent across the task periods (pre-movement: 25%; CI, [16%, 32%]; movement: 26%; CI, [19%, 31%]; *t* test; $p = 0.78$; Figure 5C). In contrast, a strict interpretation of the null space hypothesis would predict that communication from RFA to CFA cancels out on the postsynaptic side during the pre-movement phase, thus causing no change in CFA activity (Figure S5F). According to that logic, inhibiting RFA neurons projecting to the CFA should have a significantly smaller effect on the CFA population during the pre-movement phase compared to the movement phase.

As RFA-CFA communication was not consistent with a strict interpretation of the null space hypothesis, we analyzed the effects of RFA inhibition on CFA in more detail. In line with our finding that RFA projects to both inhibitory and excitatory neurons in CFA, we found that inhibiting RFA projecting neurons resulted in both enhanced and suppressed activity in CFA neurons (Figure 5D). Interestingly, in the pre-movement period, the number of enhanced and suppressed neurons was balanced (enhanced 12%; CI, [7.5%, 18%] vs. suppressed 12%; CI, [6%, 19%]; *t* test; $p = 0.9$), while more neurons were suppressed than enhanced in the movement period (enhanced 6%; CI, [2%, 10%] vs. suppressed 20%; CI, [14%, 26%]; *t* test; $p = 0.01$), indicating a switch from a balanced to a net excitatory effect of the RFA input in CFA (Figure 5E). In addition, we observed almost a complete reconfiguration of how neurons were affected by the RFA input across task phases. The majority of CFA neurons that were affected by RFA during the pre-movement phase was unaffected in the movement phase and vice versa (Figure 5F). In addition, the modulation profiles in both task phases differed from manipulations during spontaneous, out-of-task behavior (Figures S5A–S5E). Could the switch of RFA effect on CFA be related to the switch from movement-null to movement-potent spaces on the population level? To test this hypothesis, we performed a principal-component analysis of

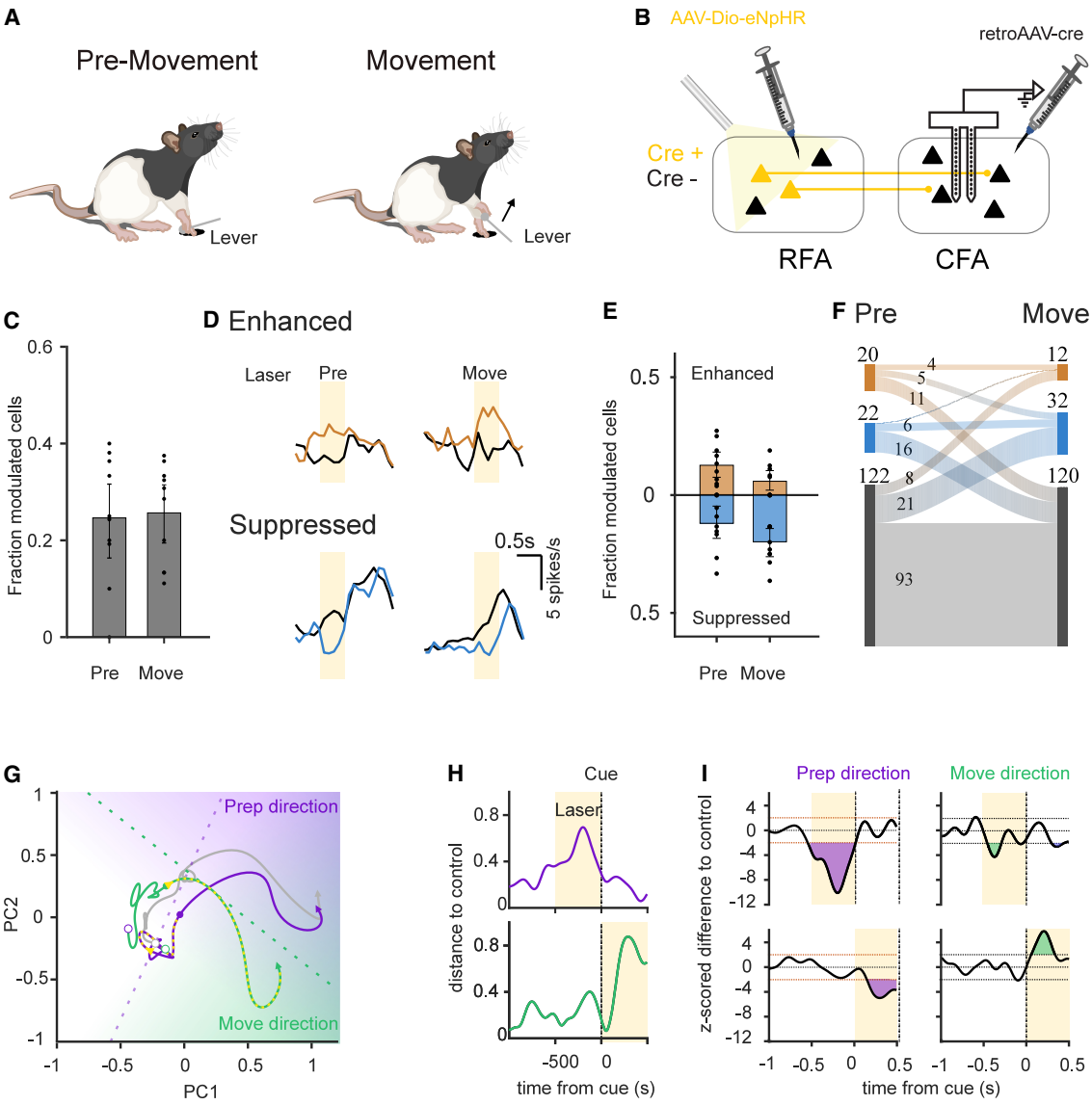

Figure 5. Reorganization of RFA influence on CFA activity from preparation to movement

(A) Schematics of behavioral task phases.

(B) Schematic of experimental strategy. AAV-Dio-eNpHR-eYFP was injected bilaterally into the RFA, and a retrograde viral vector carrying cre recombinase (retroAAV-cre) was injected into the CFA. Optical fibers were implanted bilaterally into the RFA, and a silicon probe was implanted into the CFA (N = 3 rats).

(C) Fraction of CFA neurons modulated by inhibiting RFA during the pre-movement or movement period. Error bars represent 95% confidence intervals.

(D) Weighted bootstrapped averages of neurons that are enhanced when inhibiting RFA (top) or suppressed when inhibiting RFA (bottom) during pre-movement (n = 20 and n = 22, N = 3 rats) or movement (n = 12 and n = 32, N = 3 rats).

(E) Fraction of neurons that are suppressed or enhanced when inhibiting RFA in the different task periods. Error bars represent 95% confidence intervals.

(F) Sankey plot illustrating the reorganization of CFA neurons influenced by RFA input.

(G) Output-null population activity in the first principal-component analysis plane in control trials (gray), trials with inhibition in pre-movement period (purple), and trials with inhibition in movement period (green). Laser stimulation periods are overlaid as dotted yellow lines with stimulation onset indicated by yellow arrows. Filled circles indicate cue onset.

(H) Euclidean distance in the first principal-component analysis plane between optogenetic manipulations and control conditions.

(I) Normalized difference between inhibition trials and control trials projected onto the prep direction (left) and movement direction (right) for manipulations during the pre-movement (top) and movement phases (bottom). Laser stimulation times are indicated with yellow bars.

See also Figure S5.

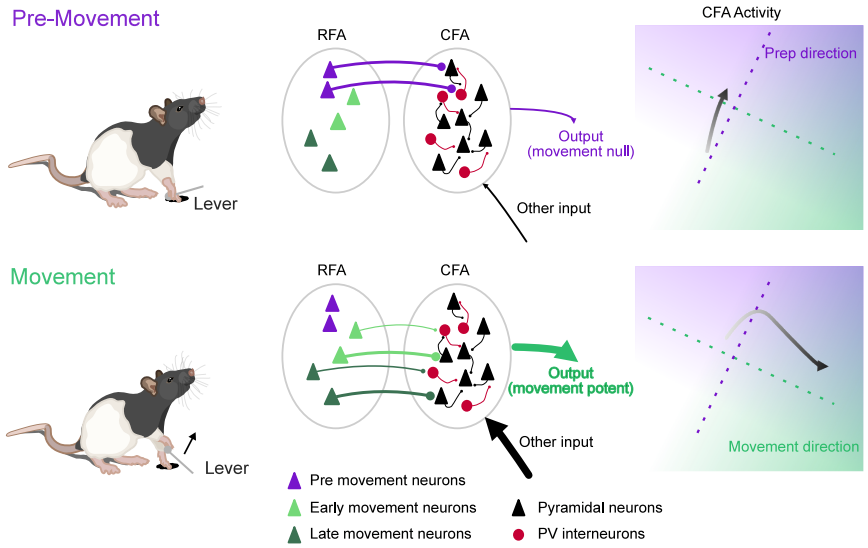

Figure 6. The switching population hypothesis

Reconfiguration of neuronal activity in RFA and CFA across preparation and movement occurs at multiple levels: Largely distinct neuronal populations in RFA engage during preparation and movement. This reconfiguration leads to a change in synaptic drive on different sets of neurons in CFA with inhibitory and excitatory neurons activated to different degrees, depending on the task phase: During the preparation phase, the excitatory and inhibitory effect of RFA on CFA is balanced and movement-null, moving CFA activity along the preparation direction in neural space. During the movement phase, the excitatory effect dominates. This change in affected CFA populations is integrated with additional input (black arrow) and coincides with the transition from movement-null to movement-potent population activity in CFA, ultimately leading to movement initiation.

the population activity of modulated neurons (Figures 5G and 5H). In control trials, i.e., without laser stimulation, activity in the first component plane developed largely into one direction during the pre-movement period, which we defined as the preparation direction (movement-null). In line with the previous finding that the movement-null and movement-potent directions are orthogonal,[17,46] the trajectory after the cue mostly traversed into the orthogonal direction, defined as movement-potent. Perturbation of RFA input during both the preparation and the movement periods caused trajectories to diverge from the control trajectory transiently during the perturbation before converging back to control conditions after the perturbation (Figures 5G and 5H), The manipulation during the pre-movement period affected activity mostly in the preparation direction (Figure 5I, upper panels). Thus, rather than being output-null with respect to CFA, in which case RFA activity should cancel out and cause no net effect, RFA pushes CFA along its own preparation (movement-null) space during the preparation phase. Manipulation during the movement period affected both preparation and movement direction (Figure 5I, lower panels). Thus, RFA output to CFA is movement-null but not output-null: during preparation, RFA does send information to CFA that does not cancel out (hence it is not output-null relative to CFA). However, this information acts along the preparation dimension of CFA, thereby remaining movement-null. In other words, RFA is output-potent in relation to CFA across the entire task but affects CFA only during the movement phase along its movement-potent direction.

Taken together, there is a major reorganization of RFA influence onto CFA during the transition from preparation to movement, while the total number of affected neurons remains constant. We, therefore, propose an updated hypothesis of premotor-motor cortex interaction during the pre-movement to movement transition (Figure 6), which we call the switching population hypothesis. Based on this framework, we put forward a number of testable hypotheses. (1) The balanced influence during movement preparation is due to the balanced activation of PV interneurons and pyramidal neurons with premotor RFA neurons targeting CFA inhibitory and excitatory neurons. The effect of this RFA population on CFA is largely along the preparation direction. (2) During movement, premotor neurons in RFA are largely silent, and instead, early and late movement neurons become active. This switch changes how individual neurons in CFA are affected by RFA and leads to a largely excitatory effect on CFA. This change in RFA to CFA influence prepares the ground for additional input, like from the thalamus,[47–51] to generate local CFA dynamics that produce activity along the movement-potent direction and cause movement.

DISCUSSION

Here, we investigated the neuronal activity in the RFA and CFA and the impact of RFA input on the CFA during different behavioral phases of prepared movements. Thereby, we established a link between neural circuit elements and the null space hypothesis.

Neuronal activity prior to movement differed between both areas with the RFA displaying more prominent pre-movement activity, in line with a role in movement preparation. The RFA conveys its pre-movement activity via direct projections to CFA where it suppresses and excites CFA units to a similar extent during movement preparation. The suppression is most

likely conveyed through direct RFA projections onto CFA PV interneurons and might serve to prevent the activity in the CFA from changing in a movement-potent direction. During movement, the impact of the RFA on the CFA switched to being mostly excitatory and influenced the neural state space along both preparation and movement-potent direction. We summarized this reorganization conceptually in our switching population hypothesis (Figure 6), which not only combines features from the null space and the gating hypothesis but also differs in important ways: in contrast to the inhibitory gating hypothesis,[12] our switching hypothesis does not require a disinhibition, in which individual PV interneurons "switch off" during movement. We predict active inputs onto PV interneurons during both preparation and movement. The balance between inputs onto excitatory and inhibitory circuits could determine whether the compound converging input onto single cells in CFA results in a net enhancing or suppressing effect. However, the interneurons might play a dual role in implementing both a partial null space by sign inversion of parts of the RFA pre-movement activity (so that these inputs would cancel out on the single-cell level) and confining the influence on CFA along the preparation direction. The finding that a similar fraction of neurons in CFA is influenced by the RFA during pre-movement and movement phases is probably the largest deviation from the null space prediction because it shows that the input during the pre-movement phase does not cancel out. Rather, the RFA input influences the CFA along its own movement-null direction during pre-movement, providing a potential mechanism of how preparation activity can be transferred between regions. Interestingly, this influence changes during movement, where the RFA also impacts the movement-potent direction. Along with these population-level changes, the CFA neurons affected by RFA input switched between task phases. This switch could mean that the communication subspace between the two areas is not only defined by which subpopulations transfer information to CFA but also by which neurons in the CFA are targeted by the RFA subpopulations.[52] These findings represent an intuitive neural mechanism underlying the change from movement-null to movement-potent spaces in CFA by associating distinct neural elements to the task phases that explain the switch.

Of course, RFA and CFA do not work in isolation.[53] Instead, brain-wide mechanisms have been revealed underlying the persistent preparatory activity in mouse premotor areas during a sensory delayed response task.[48,54–58] Similar distributed processes might also contribute to the generation of pre-movement activity in our task and combine with intrinsic cortical dynamics[59] to lead to the reconfiguration of activity between pre-movement and movement. These distributed circuits might also lead to the fast recovery of activity in CFA after perturbing RFA input. One potential candidate to induce the switch from pre-movement to movement is thalamocortical input, which has been shown to be driving cortical dynamics throughout movement.[49] In addition, thalamic input to the CFA can initiate either learned or more random forelimb movements depending on behavioral context.[50] One possibility is, therefore, that RFA primes CFA to set the initial conditions prior to movement so that thalamic input can effectively trigger the appropriate CFA dynamics and movement.

Within the framework of the switching hypothesis, we made four major contributions to the field.

First, we now close the knowledge gap of what kind of information is conveyed from the RFA to the CFA during the distinct phases of motor preparation and movement execution and how RFA affects CFA activity during these different epochs. Depending on the task phase and the subpopulations that are active in the RFA, RFA inputs engage inhibitory and excitatory neurons in the CFA to different extents to modulate local recurrent circuits.

Second, we identified a strong connection between RFA and CFA PV interneurons using immunohistochemistry and electron microscopy. Previously, it has been shown that RFA neurons project to PV interneurons in CFA[60] and that these interneurons are activated prior to the forelimb reaching movements,[14,51] suggesting a role for PV interneurons in shaping motor cortical output.[15] The high activity of the pre-movement subpopulation projecting from RFA to CFA and the relatively low firing rate in the CFA movement subpopulation during the pre-movement period suggest that PV interneurons may balance incoming excitation in the CFA during the pre-movement period. This assigns the RFA a major role in inhibiting involuntary movements by influencing CFA local circuits during pre-movement.

Third, we showed that disrupting the communication between RFA and CFA by silencing RFA to CFA projections has a similar behavioral effect as silencing either RFA or CFA on its own. This finding emphasizes the importance of corticocortical connections during movement planning. In addition, the communication between the two areas together with the convergence of information in subcortical target structures[22] could explain why manipulating RFA and CFA has often been found to have similar behavioral effects during movement preparation and execution.[32]

Fourth, we introduced and applied an innovative machine learning-based tool (NeuRL), which allows for both decoding and for the generation of predictions about neuronal subpopulations. Analogous to the reward system in animals,[61] NeuRL finds an optimal strategy based on a feedback signal. While common decoding methods rely on supervised learning without accounting for the long-term consequences of the actions, NeuRL can explicitly assign a policy that maximizes reward over time, thereby implementing an internal model of the task.[43] In contrast to previous approaches,[62,63] we thus employed inverse reinforcement learning, which extracted reward values from the rat behavior instead of regular forward reinforcement learning, which assumes the feedback signal to be known *a priori*. This approach allowed us to assign functional meaning to neuronal subpopulations by conducting simulated inhibition studies based on a modified reward function inferred from the perturbed features. Integrating this knowledge about the role of specific subpopulations into a complete virtual rodent model holds the potential of adding physiological details leading to even more powerful predictions.[64]

Moving to more complex scenarios, it will be of high interest to test how specific to an individual movement type our population switching hypothesis is or how activity would develop during a movement sequence.[65,66] In a multidirectional task, we should be able to observe whether the switch is more interpretable as a general "ready" and "go" signal related to the strong condition

invariant movement initiation signal that is observed across species in rodents[67] and non-human primates[68] or if it is specific to the type of movement that is executed. Further, probing the roles of the subpopulations with targeted interventions via optogenetic holography guided by NeuRL predictions will enable real-time functional dissection of neuronal subpopulations.[69–71]

NeuRL could also be used for future translation of our results to clinical applications. It solely requires extracellular neuronal measurements—a technique that was established in the 1950s and developed continuously in human patients up to modern high-density probes.[72–77] The newly gained knowledge about the role of specific neuronal ensembles could be incorporated into the design principles of modern brain-computer interfaces[78–85] to enhance the control of external devices and sensory write in.[86]

Limitations of the study

We employed a behavioral paradigm in which the rats initiated each trial by moving and holding a lever, analogous to the hold-and-reach tasks widely used to study preparatory activity in primates, where animals maintain the hand at a central position before executing cued outward reaches.[17,18,87] A caveat shared by these paradigms is that neural activity related to maintaining posture can be difficult to disentangle from activity reflecting movement preparation, even though RFA and CFA inhibition has already been indicated to have no effect in holding a posture but in initiating movements[88] with the additional caveat of the required force during the preparation period in our task. Future studies without required force and using temporally more precise perturbations at defined time points during the holding phase, ideally within task designs that allow for a larger number of trials per session, should help to better resolve these processes.

A second limitation is the relatively low behavioral performance of the rats, reflecting the difficulty of the task. Potentially related to the low behavioral performance, the NeuRL model did not fully capture the release time distributions of the control behavior or the effects of optogenetic manipulations. Another contributing factor may be the relatively coarse temporal resolution of the simulations (200-ms bin size). In addition, the electrophysiological dataset likely undersamples the relevant neuronal population, such that model simulations were constrained by a limited number of recorded neurons. Future work incorporating larger-scale recordings and finer temporal resolution is expected to improve model performance and alignment with empirical data.

Finally, we cannot determine the fraction of CFA PV interneurons targeted by RFA inputs. A comprehensive characterization of these inputs would ideally combine quantitative approaches, including *in vitro* synaptic connectivity analyses and volumetric electron microscopy, to more precisely assess synapse number, strength, and spatial distribution onto PV interneurons in CFA. Moreover, our electron microscopy (EM) data do not allow us to distinguish between silent and functional synapses. Nevertheless, when considered together with the *in vivo* manipulation results, the most parsimonious interpretation is that these synapses are functionally relevant and contribute to the switching from preparation to movement.

RESOURCE AVAILABILITY

Lead contact

Further information and requests for resources and reagents should be directed to and will be fulfilled by the lead contact, Ilka Diester (ilka.diester@biologie.uni-freiburg.de).

Materials availability

This study did not generate new unique reagents.

Data and code availability

- All original code has been deposited under DOI: 10.5281/zenodo.20071317 and is publicly available as of the date of publication.
- Data reported in this paper will be shared by the lead contact upon request.
- Any additional information required to reanalyze the data reported in this paper is available from the lead contact upon request.

ACKNOWLEDGMENTS

We would like to thank Sigrun Nestel for technical assistance in electron microscopy and Dan O'Shea and Andreas Draguhn for comments on an earlier version of this manuscript. We thank Zongpeng Sun, Philippe Coulon, and Brice de la Crompe for discussions about the experimental design, follow-up experiments, and data interpretation, respectively. We thank Etienne Ackermann and scidraw.io for the illustrations. This work was supported as part of BrainLinks-BrainTools, which is funded by the Federal Ministry of Economics, Science and Arts of Baden-Württemberg within the sustainability program for projects of the Excellence Initiative II, by the Bernstein Award 2012 (01GQ2301); the Deutsche Forschungsgemeinschaft (DFG) via grants DI 1908/3-1, DI 1908/11-1, DI 1908/12-1, DI1908/16-1, and DI 1908/6-1; I.D.'s subprojects within the CRC1690 and RU5159; and the ERC Starting Grant OptoMotorPath (338041), which were all awarded to I.D., and the subprojects of I.D., J.B., and A.V. of the DFG CRC/TRR 384 and DFG AM 443/3-1, which was awarded to J.A.

AUTHOR CONTRIBUTIONS

I.D. and J.B. conceived the study. J.J.A, M.A., I.D., G. Kalweit, H.Z., J.B., and A.V. wrote the manuscript. M.A. performed all *in vivo* experiments. M.A. and J.J.A. and H.Z. performed the data analysis. G. Kalweit, M.K., H.Z., and J.B. designed the Q-learning approach. G. Kalweit, M.K., and H.Z. performed the *in silico* experiments. G. Karvat designed and built the electrophysiological and behavioral setup. A.S. and Z.J. supported the histological evaluations. C.A. supported visualization. A.A. supported the confocal imaging and the viral tracing and slicing for the EM, M.D.D. and Y.T. supported viral tracing for the EM, A.V. contributed the EM, I.D. and J.B. supervised the project, and I.D., J.B., and J.A. took care of the funding acquisition.

DECLARATION OF INTERESTS

The authors declare no competing interests.

STAR★METHODS

Detailed methods are provided in the online version of this paper and include the following:

- KEY RESOURCES TABLE
- EXPERIMENTAL MODEL AND STUDY PARTICIPANT DETAILS
  - Animals
- METHOD DETAILS
  - Behavioral setup
  - Behavioral training
  - Stereotaxic injections and implantation sites
  - Data acquisition
- QUANTIFICATION AND STATISTICAL ANALYSIS

- Behavior
- Electropysiology
- Histology
- Electron microscopy
- Statistical tests
- Decoding lever position from neural activities
- Inverse reinforcement learning

SUPPLEMENTAL INFORMATION

Supplemental information can be found online at https://doi.org/10.1016/j.celrep.2026.117542.

Received: March 14, 2025
Revised: January 30, 2026
Accepted: May 25, 2026

REFERENCES

1. Ferrier, D., and Burdon-Sanderson, J.S. (1875). Experiments on the brain of monkeys.—No. I. Proc. R. Soc. Lond. *23*, 409–430. https://doi.org/10.1098/rspl.1874.0058.
2. Fritsch, G., and Hitzig, E. (2009). Electric excitability of the cerebrum (Uber die elektrische Erregbarkeit des Grosshirns). Epilepsy Behav. *15*, 123–130. https://doi.org/10.1016/j.yebeh.2009.03.001.
3. Tanji, J., and Evarts, E.V. (1976). Anticipatory activity of motor cortex neurons in relation to direction of an intended movement. J. Neurophysiol. *39*, 1062–1068. https://doi.org/10.1152/jn.1976.39.5.1062.
4. Weinrich, M., Wise, S.P., and Mauritz, K.H. (1984). A neurophysiological study of the premotor cortex in the rhesus monkey. Brain *107*, 385–414. https://doi.org/10.1093/brain/107.2.385.
5. Churchland, M.M., Santhanam, G., and Shenoy, K.V. (2006). Preparatory activity in premotor and motor cortex reflects the speed of the upcoming reach. J. Neurophysiol. *96*, 3130–3146. https://doi.org/10.1152/jn.00307.2006.
6. Churchland, M.M., Yu, B.M., Ryu, S.I., Santhanam, G., and Shenoy, K.V. (2006). Neural Variability in Premotor Cortex Provides a Signature of Motor Preparation. J. Neurosci. *26*, 3697–3712. https://doi.org/10.1523/JNEUROSCI.3762-05.2006.
7. Crammond, D.J., and Kalaska, J.F. (2000). Prior Information in Motor and Premotor Cortex: Activity During the Delay Period and Effect on Pre-Movement Activity. J. Neurophysiol. *84*, 986–1005. https://doi.org/10.1152/jn.2000.84.2.986.
8. Riehle, A., and Requin, J. (1989). Monkey primary motor and premotor cortex: single-cell activity related to prior information about direction and extent of an intended movement. J. Neurophysiol. *61*, 534–549. https://doi.org/10.1152/jn.1989.61.3.534.
9. Churchland, M.M., and Shenoy, K.V. (2007). Delay of Movement Caused by Disruption of Cortical Preparatory Activity. J. Neurophysiol. *97*, 348–359. https://doi.org/10.1152/jn.00808.2006.
10. Soteropoulos, D.S. (2018). Corticospinal gating during action preparation and movement in the primate motor cortex. J. Neurophysiol. *119*, 1538–1555. https://doi.org/10.1152/jn.00639.2017.
11. Turner, R.S., and DeLong, M.R. (2000). Corticostriatal Activity in Primary Motor Cortex of the Macaque. J. Neurosci. *20*, 7096–7108. https://doi.org/10.1523/JNEUROSCI.20-18-07096.2000.
12. Bullock, D., and Grossberg, S. (1988). Neural dynamics of planned arm movements: emergent invariants and speed-accuracy properties during trajectory formation. Psychol. Rev. *95*, 49–90. https://doi.org/10.1037/0033-295x.95.1.49.
13. Kaufman, M.T., Churchland, M.M., and Shenoy, K.V. (2013). The roles of monkey M1 neuron classes in movement preparation and execution. J. Neurophysiol. *110*, 817–825. https://doi.org/10.1152/jn.00892.2011.
14. Estebanez, L., Hoffmann, D., Voigt, B.C., and Poulet, J.F.A. (2017). Parvalbumin-Expressing GABAergic Neurons in Primary Motor Cortex Signal Reaching. Cell Rep. *20*, 308–318. https://doi.org/10.1016/j.celrep.2017.06.044.
15. Isomura, Y., Harukuni, R., Takekawa, T., Aizawa, H., and Fukai, T. (2009). Microcircuitry coordination of cortical motor information in self-initiation of voluntary movements. Nat. Neurosci. *12*, 1586–1593. https://doi.org/10.1038/nn.2431.
16. Churchland, M.M., and Shenoy, K.V. (2024). Preparatory activity and the expansive null-space. Nat. Rev. Neurosci. *25*, 213–236. https://doi.org/10.1038/s41583-024-00796-z.
17. Elsayed, G.F., Lara, A.H., Kaufman, M.T., Churchland, M.M., and Cunningham, J.P. (2016). Reorganization between preparatory and movement population responses in motor cortex. Nat. Commun. *7*, 13239. https://doi.org/10.1038/ncomms13239.
18. Kaufman, M.T., Churchland, M.M., Ryu, S.I., and Shenoy, K.V. (2014). Cortical activity in the null space: permitting preparation without movement. Nat. Neurosci. *17*, 440–448. https://doi.org/10.1038/nn.3643.
19. Neafsey, E.J., and Sievert, C. (1982). A second forelimb motor area exists in rat frontal cortex. Brain Res. *232*, 151–156. https://doi.org/10.1016/0006-8993(82)90617-5.
20. Kreis, S.L., Luhmann, H.J., Ciolac, D., Groppa, S., and Muthuraman, M. (2022). Translational Model of Cortical Premotor-Motor Networks. Cereb. Cortex *32*, 2621–2634. https://doi.org/10.1093/cercor/bhab369.
21. Lazari, A., Tachrount, M., Valverde, J.M., Papp, D., Beauchamp, A., McCarthy, P., Ellegood, J., Grandjean, J., Johansen-Berg, H., Zerbi, V., et al. (2024). The mouse motor system contains multiple premotor areas and partially follows human organizational principles. Cell Rep. *43*, 114191. https://doi.org/10.1016/j.celrep.2024.114191.
22. Rouiller, E.M., Moret, V., and Liang, F. (1993). Comparison of the Connectional Properties of the Two Forelimb Areas of the Rat Sensorimotor Cortex: Support for the Presence of a Premotor or Supplementary Motor Cortical Area. SMR (Somatosens. Mot. Res.) *10*, 269–289. https://doi.org/10.3109/08990229309028837.
23. Urban III, E.T., Hudson, H.M., Li, Y., Nishibe, M., Barbay, S., Guggenmos, D.J., and Nudo, R.J. (2024). Corticocortical connections of the rostral forelimb area in rats: a quantitative tract-tracing study. Cereb. Cortex *34*, bhad530. https://doi.org/10.1093/cercor/bhad530.
24. Soma, S., Saiki, A., Yoshida, J., Ríos, A., Kawabata, M., Sakai, Y., and Isomura, Y. (2017). Distinct Laterality in Forelimb-Movement Representations of Rat Primary and Secondary Motor Cortical Neurons with Intratelencephalic and Pyramidal Tract Projections. J. Neurosci. *37*, 10904–10916. https://doi.org/10.1523/JNEUROSCI.1188-17.2017.
25. Carmona, L.M., Thomas, E.D., Smith, K., Tasic, B., Costa, R.M., and Nelson, A. (2024). Topographical and cell type-specific connectivity of rostral and caudal forelimb corticospinal neuron populations. Cell Rep. *43*, 113993. https://doi.org/10.1016/j.celrep.2024.113993.
26. Wang, X., Liu, Y., Li, X., Zhang, Z., Yang, H., Zhang, Y., Williams, P.R., Alwahab, N.S.A., Kapur, K., Yu, B., et al. (2017). Deconstruction of Corticospinal Circuits for Goal-Directed Motor Skills. Cell *171*, 440–455.e14. https://doi.org/10.1016/j.cell.2017.08.014.
27. Tennant, K.A., Adkins, D.L., Donlan, N.A., Asay, A.L., Thomas, N., Kleim, J.A., and Jones, T.A. (2011). The Organization of the Forelimb Representation of the C57BL/6 Mouse Motor Cortex as Defined by Intracortical Microstimulation and Cytoarchitecture. Cereb. Cortex *21*, 865–876. https://doi.org/10.1093/cercor/bhq159.
28. Brown, A.R., Mitra, S., Teskey, G.C., and Boychuk, J.A. (2023). Complex forelimb movements and cortical topography evoked by intracortical microstimulation in male and female mice. Cereb. Cortex *33*, 1866–1875. https://doi.org/10.1093/cercor/bhac178.
29. Hira, R., Ohkubo, F., Ozawa, K., Isomura, Y., Kitamura, K., Kano, M., Kasai, H., and Matsuzaki, M. (2013). Spatiotemporal Dynamics of Functional Clusters of Neurons in the Mouse Motor Cortex during a Voluntary

Movement. J. Neurosci. *33*, 1377–1390. https://doi.org/10.1523/JNEUROSCI.2550-12.2013.

30. Kimura, R., Saiki, A., Fujiwara-Tsukamoto, Y., Sakai, Y., and Isomura, Y. (2017). Large-scale analysis reveals populational contributions of cortical spike rate and synchrony to behavioural functions. J. Physiol. *595*, 385–413. https://doi.org/10.1113/JP272794.
31. Saiki, A., Kimura, R., Samura, T., Fujiwara-Tsukamoto, Y., Sakai, Y., and Isomura, Y. (2014). Different modulation of common motor information in rat primary and secondary motor cortices. PLoS One *9*, e98662. https://doi.org/10.1371/journal.pone.0098662.
32. Morandell, K., and Huber, D. (2017). The role of forelimb motor cortex areas in goal directed action in mice. Sci. Rep. *7*, 15759. https://doi.org/10.1038/s41598-017-15835-2.
33. Hira, R., Ohkubo, F., Tanaka, Y.R., Masamizu, Y., Augustine, G.J., Kasai, H., and Matsuzaki, M. (2013). In vivo optogenetic tracing of functional corticocortical connections between motor forelimb areas. Front. Neural Circuits *7*, 55. https://doi.org/10.3389/fncir.2013.00055.
34. Ueta, Y., Otsuka, T., Morishima, M., Ushimaru, M., and Kawaguchi, Y. (2014). Multiple Layer 5 Pyramidal Cell Subtypes Relay Cortical Feedback from Secondary to Primary Motor Areas in Rats. Cereb. Cortex *24*, 2362–2376. https://doi.org/10.1093/cercor/bht088.
35. Saiki-Ishikawa, A., Agrios, M., Savya, S., Forrest, A., Sroussi, H., Hsu, S., Basrai, D., Xu, F., and Miri, A. (2025). Hierarchy between forelimb premotor and primary motor cortices and its manifestation in their firing patterns. eLife *13*, RP103069. https://doi.org/10.7554/eLife.103069.
36. Makino, H., Ren, C., Liu, H., Kim, A.N., Kondapaneni, N., Liu, X., Kuzum, D., and Komiyama, T. (2017). Transformation of Cortex-wide Emergent Properties during Motor Learning. Neuron *94*, 880–890.e8. https://doi.org/10.1016/j.neuron.2017.04.015.
37. Veuthey, T.L., Derosier, K., Kondapavulur, S., and Ganguly, K. (2020). Single-trial cross-area neural population dynamics during long-term skill learning. Nat. Commun. *11*, 4057. https://doi.org/10.1038/s41467-020-17902-1.
38. Omlor, W., Wahl, A.-S., Sipilä, P., Lütcke, H., Laurenczy, B., Chen, I.-W., Sumanovski, L.T., van 't Hoff, M., Bethge, P., Voigt, F.F., et al. (2019). Context-dependent limb movement encoding in neuronal populations of motor cortex. Nat. Commun. *10*, 4812. https://doi.org/10.1038/s41467-019-12670-z.
39. Terada, S.-I., Kobayashi, K., and Matsuzaki, M. (2022). Transition of distinct context-dependent ensembles from secondary to primary motor cortex in skilled motor performance. Cell Rep. *41*, 111494. https://doi.org/10.1016/j.celrep.2022.111494.
40. Karvat, G., Alyahyay, M., and Diester, I. (2021). Spontaneous activity competes with externally evoked responses in sensory cortex. Proc. Natl. Acad. Sci. USA *118*, e2023286118. https://doi.org/10.1073/pnas.2023286118.
41. Sun, Z., Schneider, A., Alyahyay, M., Karvat, G., and Diester, I. (2021). Effects of optogenetic stimulation of primary somatosensory cortex and its projections to striatum on vibrotactile perception in freely moving rats. eNeuro *8*, ENEURO.0453, 20.2021. https://doi.org/10.1523/ENEURO.0453-20.2021.
42. Kalweit, G., Kalweit, M., Alyahyay, M., Jaeckel, Z., Steenbergen, F., Hardung, S., Brox, T., Diester, I., and Boedecker, J. (2022). NeuRL: Closed-form Inverse Reinforcement Learning for Neural Decoding https://doi.org/10.48550/arXiv.2204.04733.
43. Diester, I., Bartos, M., Bödecker, J., Kortylewski, A., Leibold, C., Letzkus, J., Nour, M.M., Schönauer, M., Straw, A., Valada, A., et al. (2024). Internal world models in humans, animals, and AI. Neuron *112*, 2265–2268. https://doi.org/10.1016/j.neuron.2024.06.019.
44. Kalweit, G., Huegle, M., Werling, M., and Boedecker, J. (2020). Deep Inverse Q-learning with Constraints. In Advances in Neural Information Processing Systems, H. Larochelle, M. Ranzato, R. Hadsell, M.F. Balcan, and H. Lin, eds. (Curran Associates, Inc.), pp. 14291–14302. https://proceedings.neurips.cc/paper_files/paper/2020/file/a4c42bfd5f5130ddf96e34a036c75e0a-Paper.pdf.
45. Klemann, C.J.H.M., and Roubos, E.W. (2011). The gray area between synapse structure and function—Gray's synapse types I and II revisited. Synapse *65*, 1222–1230. https://doi.org/10.1002/syn.20962.
46. Arroyo, S., Barati, S., Kim, K., Aparicio, F., and Ganguly, K. (2023). Emergence of preparatory dynamics in VIP interneurons during motor learning. Cell Rep. *42*, 112834. https://doi.org/10.1016/j.celrep.2023.112834.
47. Takahashi, N., Moberg, S., Zolnik, T.A., Catanese, J., Sachdev, R.N.S., Larkum, M.E., and Jaeger, D. (2021). Thalamic input to motor cortex facilitates goal-directed action initiation. Curr. Biol. *31*, 4148–4155.e4. https://doi.org/10.1016/j.cub.2021.06.089.
48. Zhu, J., Hasanbegović, H., Liu, L.D., Gao, Z., and Li, N. (2023). Activity map of a cortico-cerebellar loop underlying motor planning. Nat. Neurosci. *26*, 1916–1928. https://doi.org/10.1038/s41593-023-01453-x.
49. Sauerbrei, B.A., Guo, J.-Z., Cohen, J.D., Mischiati, M., Guo, W., Kabra, M., Verma, N., Mensh, B., Branson, K., and Hantman, A.W. (2020). Cortical pattern generation during dexterous movement is input-driven. Nature *577*, 386–391. https://doi.org/10.1038/s41586-019-1869-9.
50. Dacre, J., Colligan, M., Clarke, T., Ammer, J.J., Schiemann, J., Chamosa-Pino, V., Claudi, F., Harston, J.A., Eleftheriou, C., Pakan, J.M.P., et al. (2021). A cerebellar-thalamocortical pathway drives behavioral context-dependent movement initiation. Neuron *109*, 2326–2338.e8. https://doi.org/10.1016/j.neuron.2021.05.016.
51. Nashef, A., Cohen, O., Perlmutter, S.I., and Prut, Y. (2022). A cerebellar origin of feedforward inhibition to the motor cortex in non-human primates. Cell Rep. *39*, 110803. https://doi.org/10.1016/j.celrep.2022.110803.
52. Kohn, A., Jasper, A.I., Semedo, J.D., Gokcen, E., Machens, C.K., and Yu, B.M. (2020). Principles of Corticocortical Communication: Proposed Schemes and Design Considerations. Trends Neurosci. *43*, 725–737. https://doi.org/10.1016/j.tins.2020.07.001.
53. Khilkevich, A., Lohse, M., Low, R., Orsolic, I., Bozic, T., Windmill, P., and Mrsic-Flogel, T.D. (2024). Brain-wide dynamics linking sensation to action during decision-making. Nature *634*, 890–900. https://doi.org/10.1038/s41586-024-07908-w.
54. Chen, G., Kang, B., Lindsey, J., Druckmann, S., and Li, N. (2021). Modularity and robustness of frontal cortical networks. Cell *184*, 3717–3730.e24. https://doi.org/10.1016/j.cell.2021.05.026.
55. Chen, S., Liu, Y., Wang, Z.A., Colonell, J., Liu, L.D., Hou, H., Tien, N.-W., Wang, T., Harris, T., Druckmann, S., et al. (2024). Brain-wide neural activity underlying memory-guided movement. Cell *187*, 676–691.e16. https://doi.org/10.1016/j.cell.2023.12.035.
56. Gao, Z., Davis, C., Thomas, A.M., Economo, M.N., Abrego, A.M., Svoboda, K., De Zeeuw, C.I., and Li, N. (2018). A cortico-cerebellar loop for motor planning. Nature *563*, 113–116. https://doi.org/10.1038/s41586-018-0633-x.
57. Li, N., Chen, T.-W., Guo, Z.V., Gerfen, C.R., and Svoboda, K. (2015). A motor cortex circuit for motor planning and movement. Nature *519*, 51–56. https://doi.org/10.1038/nature14178.
58. Svoboda, K., and Li, N. (2018). Neural mechanisms of movement planning: motor cortex and beyond. Curr. Opin. Neurobiol. *49*, 33–41. https://doi.org/10.1016/j.conb.2017.10.023.
59. Wu, A., Chen, Q., Yu, B., Chae, S., Tan, Z., Ramot, A., and Komiyama, T. (2025). Targeted stimulation of motor cortex neural ensembles drives learned movements. Preprint at bioRxiv. https://doi.org/10.1101/2025.01.06.631504.
60. Duan, Z., Li, A., Gong, H., and Li, X. (2020). A Whole-brain Map of Long-range Inputs to GABAergic Interneurons in the Mouse Caudal Forelimb Area. Neurosci. Bull. *36*, 493–505. https://doi.org/10.1007/s12264-019-00458-6.
61. Glimcher, P.W. (2011). Understanding dopamine and reinforcement learning: The dopamine reward prediction error hypothesis. Proc.

Natl. Acad. Sci. USA *108*, 15647–15654. https://doi.org/10.1073/pnas.1014269108.

62. Botvinick, M., Wang, J.X., Dabney, W., Miller, K.J., and Kurth-Nelson, Z. (2020). Deep Reinforcement Learning and Its Neuroscientific Implications. Neuron *107*, 603–616. https://doi.org/10.1016/j.neuron.2020.06.014.

63. Gershman, S.J. (2018). The Successor Representation: Its Computational Logic and Neural Substrates. J. Neurosci. *38*, 7193–7200. https://doi.org/10.1523/JNEUROSCI.0151-18.2018.

64. Aldarondo, D., Merel, J., Marshall, J.D., Hasenclever, L., Klibaite, U., Gellis, A., Tassa, Y., Wayne, G., Botvinick, M., and Ölveczky, B.P. (2024). A virtual rodent predicts the structure of neural activity across behaviours. Nature *632*, 594–602. https://doi.org/10.1038/s41586-024-07633-4.

65. Mizes, K.G.C., Lindsey, J., Escola, G.S., and Ölveczky, B.P. (2024). The role of motor cortex in motor sequence execution depends on demands for flexibility. Nat. Neurosci. *27*, 2466–2475. https://doi.org/10.1038/s41593-024-01792-3.

66. Kristl, A.C., Koh, N., Agrios, M., Savya, S., Ma, Z., Basrai, D., Hsu, S., and Miri, A. (2025). Interactions between motor cortical forelimb regions and their influence on muscles reorganize across behaviors. Nat. Commun. *16*, 10364. https://doi.org/10.1038/s41467-025-65381-z.

67. Currie, S.P., Ammer, J.J., Premchand, B., Dacre, J., Wu, Y., Eleftheriou, C., Colligan, M., Clarke, T., Mitchell, L., Faisal, A.A., et al. (2022). Movement-specific signaling is differentially distributed across motor cortex layer 5 projection neuron classes. Cell Rep. *39*, 110801. https://doi.org/10.1016/j.celrep.2022.110801.

68. Kaufman, M.T., Seely, J.S., Sussillo, D., Ryu, S.I., Shenoy, K.V., and Churchland, M.M. (2016). The Largest Response Component in the Motor Cortex Reflects Movement Timing but Not Movement Type. eNeuro *3*, ENEURO.0085, 16.2016. https://doi.org/10.1523/ENEURO.0085-16.2016.

69. Adesnik, H., and Abdeladim, L. (2021). Probing neural codes with two-photon holographic optogenetics. Nat. Neurosci. *24*, 1356–1366. https://doi.org/10.1038/s41593-021-00902-9.

70. Packer, A.M., Russell, L.E., Dalgleish, H.W.P., and Häusser, M. (2015). Simultaneous all-optical manipulation and recording of neural circuit activity with cellular resolution in vivo. Nat. Methods *12*, 140–146. https://doi.org/10.1038/nmeth.3217.

71. Ronzitti, E., Emiliani, V., and Papagiakoumou, E. (2018). Methods for Three-Dimensional All-Optical Manipulation of Neural Circuits. Front. Cell. Neurosci. *12*, 469. https://doi.org/10.3389/fncel.2018.00469.

72. Nordhausen, C.T., Rousche, P.J., and Normann, R.A. (1994). Optimizing recording capabilities of the Utah Intracortical Electrode Array. Brain Res. *637*, 27–36. https://doi.org/10.1016/0006-8993(94)91213-0.

73. Paulk, A.C., Kfir, Y., Khanna, A.R., Mustroph, M.L., Trautmann, E.M., Soper, D.J., Stavisky, S.D., Welkenhuysen, M., Dutta, B., Shenoy, K.V., et al. (2022). Large-scale neural recordings with single neuron resolution using Neuropixels probes in human cortex. Nat. Neurosci. *25*, 252–263. https://doi.org/10.1038/s41593-021-00997-0.

74. Ulbert, I., Halgren, E., Heit, G., and Karmos, G. (2001). Multiple microelectrode-recording system for human intracortical applications. J. Neurosci. Methods *106*, 69–79. https://doi.org/10.1016/s0165-0270(01)00330-2.

75. Verzeano, M., Crandall, P.H., and Dymond, A. (1971). Neuronal activity of the amygdala in patients with psychomotor epilepsy. Neuropsychologia *9*, 331–344. https://doi.org/10.1016/0028-3932(71)90029-7.

76. Ward, A.A., and Thomas, L.B. (1955). The electrical activity of single units in the cerebral cortex of man. Electroencephalogr. Clin. Neurophysiol. *7*, 135–136. https://doi.org/10.1016/0013-4694(55)90067-5.

77. Worrell, G.A., Gardner, A.B., Stead, S.M., Hu, S., Goerss, S., Cascino, G.J., Meyer, F.B., Marsh, R., and Litt, B. (2008). High-frequency oscillations in human temporal lobe: simultaneous microwire and clinical macroelectrode recordings. Brain *131*, 928–937. https://doi.org/10.1093/brain/awn006.

78. Chestek, C.A., Gilja, V., Nuyujukian, P., Foster, J.D., Fan, J.M., Kaufman, M.T., Churchland, M.M., Rivera-Alvidrez, Z., Cunningham, J.P., Ryu, S.I., and Shenoy, K.V. (2011). Long-term stability of neural prosthetic control signals from silicon cortical arrays in rhesus macaque motor cortex. J. Neural. Eng. *8*, 045005. https://doi.org/10.1088/1741-2560/8/4/045005.

79. Flesher, S.N., Collinger, J.L., Foldes, S.T., Weiss, J.M., Downey, J.E., Tyler-Kabara, E.C., Bensmaia, S.J., Schwartz, A.B., Boninger, M.L., and Gaunt, R.A. (2016). Intracortical microstimulation of human somatosensory cortex. Sci. Transl. Med. *8*, 361ra141. https://doi.org/10.1126/scitranslmed.aaf8083.

80. Hochberg, L.R., Bacher, D., Jarosiewicz, B., Masse, N.Y., Simeral, J.D., Vogel, J., Haddadin, S., Liu, J., Cash, S.S., van der Smagt, P., and Donoghue, J.P. (2012). Reach and grasp by people with tetraplegia using a neurally controlled robotic arm. Nature *485*, 372–375. https://doi.org/10.1038/nature11076.

81. Hochberg, L.R., Serruya, M.D., Friehs, G.M., Mukand, J.A., Saleh, M., Caplan, A.H., Branner, A., Chen, D., Penn, R.D., and Donoghue, J.P. (2006). Neuronal ensemble control of prosthetic devices by a human with tetraplegia. Nature *442*, 164–171. https://doi.org/10.1038/nature04970.

82. Stavisky, S.D., Willett, F.R., Avansino, D.T., Hochberg, L.R., Shenoy, K.V., and Henderson, J.M. (2020). Speech-related dorsal motor cortex activity does not interfere with iBCI cursor control. J. Neural. Eng. *17*, 016049. https://doi.org/10.1088/1741-2552/ab5b72.

83. Stavisky, S.D., Willett, F.R., Wilson, G.H., Murphy, B.A., Rezaii, P., Avansino, D.T., Memberg, W.D., Miller, J.P., Kirsch, R.F., Hochberg, L.R., et al. (2019). Neural ensemble dynamics in dorsal motor cortex during speech in people with paralysis. eLife *8*, e46015. https://doi.org/10.7554/eLife.46015.

84. Willett, F.R., Avansino, D.T., Hochberg, L.R., Henderson, J.M., and Shenoy, K.V. (2021). High-performance brain-to-text communication via handwriting. Nature *593*, 249–254. https://doi.org/10.1038/s41586-021-03506-2.

85. Willsey, M.S., Nason-Tomaszewski, S.R., Ensel, S.R., Temmar, H., Mender, M.J., Costello, J.T., Patil, P.G., and Chestek, C.A. (2022). Real-time brain-machine interface in non-human primates achieves high-velocity prosthetic finger movements using a shallow feedforward neural network decoder. Nat. Commun. *13*, 6899. https://doi.org/10.1038/s41467-022-34452-w.

86. Flesher, S.N., Downey, J.E., Weiss, J.M., Hughes, C.L., Herrera, A.J., Tyler-Kabara, E.C., Boninger, M.L., Collinger, J.L., and Gaunt, R.A. (2021). A brain-computer interface that evokes tactile sensations improves robotic arm control. Science *372*, 831–836. https://doi.org/10.1126/science.abd0380.

87. Churchland, M.M., Cunningham, J.P., Kaufman, M.T., Ryu, S.I., and Shenoy, K.V. (2010). Cortical preparatory activity: representation of movement or first cog in a dynamical machine? Neuron *68*, 387–400. https://doi.org/10.1016/j.neuron.2010.09.015.

88. Bollu, T., Whitehead, S.C., Prasad, N., Walker, J., Shyamkumar, N., Subramaniam, R., Kardon, B., Cohen, I., and Goldberg, J.H. (2024). Motor cortical inactivation impairs corrective submovements in mice performing a hold-still center-out reach task. J. Neurophysiol. *132*, 829–848. https://doi.org/10.1152/jn.00241.2023.

89. Pachitariu, M., Steinmetz, N., Kadir, S., Carandini, M., and D, H.K. (2016). Kilosort: realtime spike-sorting for extracellular electrophysiology with hundreds of channels. Preprint at bioRxiv. https://doi.org/10.1101/061481.

90. Churchland, M.M., Cunningham, J.P., Kaufman, M.T., Foster, J.D., Nuyujukian, P., Ryu, S.I., and Shenoy, K.V. (2012). Neural population dynamics during reaching. Nature *487*, 51–56. https://doi.org/10.1038/nature11129.

91. Lu, H., Yang, B., and Jaeger, D. (2016). Cerebellar Nuclei Neurons Show Only Small Excitatory Responses to Optogenetic Olivary Stimulation in Transgenic Mice: In Vivo and In Vitro Studies. Front. Neural Circuits *10*, 21.

STAR★METHODS

KEY RESOURCES TABLE

REAGENT or RESOURCE	SOURCE	IDENTIFIER
Antibodies		
anti-Parvalbumin	Merck Millipore	P3088; RRID: AB_15736
anti-Parvalbumin	Swant	PV235; RRID: AB_3698492
Cy3 goat anti-mouse	Thermofisher	M30010; RRID: AB_1181146
GFP polyclonal antibody	Thermofisher	A11122; RRID: AB_221569
Nanogold 1.4 nm goat anti-rabbit	Biotrend	–
biotinylated anti-mouse	Vector	–
Bacterial and virus strains		
rAAV5/hSyn-hChR2(H134R)-eYFP-WPREpA	Karl Deisseroth	RRID: Addgene_26973
rAAV5/hSyn-eNpHR3.0-eYFP	Karl Deisseroth	RRID: Addgene: 26972
rAAV5/EF1a-DIO-eNpHR3.0-eYFP	Karl Deisseroth	RRID: Addgene: 26966
rAAV2-retro.CAG-Cre	Edward Boyden	RRID: Addgene: 196140-AAVrg
Chemicals, peptides, and recombinant proteins		
Durcupan A/M (100 mL)	Sigma	–
Durcupan B (100 mL)	Sigma	–
Durcupan C	Sigma	–
Durcupan D	Sigma	–
Formaldehyd, 16%, MeOHfrei, 10 × 10mL	Polysciences	–
Glutaraldehyd 25% 10 x 10mL	science	–
HQ Silver Initiator/Moderator/Activator	Biotrend Chemikalien GmbH	–
Experimental models: Organisms/strains		
Rat: CD Sprague Dawley	Charles River	001
Software and algorithms		
MATLAB versions R2018b and R2024a	Mathworks	https://www.mathworks.com/products/matlab.html
Python 3.10.13	Python	Python.org
Custom code	–	Zenodo: https://doi.org/10.5281/zenodo.20071317
KiloSort	Ref. [89]	https://doi.org/10.1101/061481
jPCA	Ref. [90]	https://doi.org/10.1038/nature11129
RPvdsEx	Tucker Davis Technologies	https://www.tdt.com/product/rpvdsex/
OpenEX software suite	Tucker Davis Technologies	https://www.tdt.com/product/openex-software-suite/
Med-PC software	Med Associates	https://med-associates.com/product/med-pc/
ImageSP	Tröndle, Germany	–
Other		
Digital headstage	Tucker Davis Technologies	ZD32
Electrophysiological recording system	Tucker Davis Technologies	RZ2 bioamp
Electrodes	Atlas Neuroengineering	E32+R-150-S2-L6-200 NT
Behavioral control	Med Associates	Med-PC

EXPERIMENTAL MODEL AND STUDY PARTICIPANT DETAILS

Animals

Female adult CD IGS rats (Sprague Dawley; 15 rats; 8 weeks of age; 250–300 g) were used in this study. They were group-housed (2–4 per group) in IVC cages of Type IV 1500 U (Blueline Series from Tecniplast, Germany) under a reversed 12 h light-dark cycle (light off from 8 a.m. to 8 p.m., for the duration of the training and experiments). One week before the first behavioral training, rats were

handled daily. Food (standard lab chow) and water were provided *ad libitum*. During the course of the experiment, free access to food was maintained but water was restricted while keeping the rats at > 85% of their weight before water restriction. For 2 days per week, *ad libitum* food and water access were ensured. All animal procedures (surgeries, behavioral training, optogenetics, electrophysiological recordings, and perfusions) were approved by the Regierungspräsidium Freiburg, Germany (animal license numbers G-15/011, G-20/026 and G-20/97).

METHOD DETAILS

Behavioral setup

We employed a preparation-movement task for freely moving rats.[40] The early training process employed four custom-built setups, each individually controlled using Med-PC software to enable simultaneous training (Med Associates, Fairfax, VT). Each training box included a 30 × 25 × 30 cm plexiglass box with a grounded metal floor. A 2 × 12 mm infusion cannula (1464LL, Acufirm, Dreieich, Germany) covered with a 7 mm (diameter) metal ball served as a lever. The lever was clamped to a holder 1 cm above the cage ground and between two 65 × 35 mm retractable plexiglass walls. The holder was centered by two pairs of magnets (adhesive force 2.5 kg, model S-08-08-N, Supermagnete, Gottmadingen, Germany). We controlled the distance between magnets, and thus their force, by attaching them to M12 screws. The axis of the holder was connected to a 10-bit magnetic angle encoder (AEAT-6010, Avago Technologies, San Jose, CA) reporting the left-right position. The metal holder was connected to a 5V power source, thus forming a conductive touch sensor. To deliver vibrotactile stimuli, we glued a small vibrating motor (3V ERM motor, Digikey no. 1597-1244-ND, Seeed Technology Co., Shenzhen, China) to the lever. The vibrator, touch sensor, and angle encoder were controlled by an Arduino Uno (Arduino, Turin, Italy) connected via transistor-transistor-logic (TTL) to the Med Associates control cabinet. We controlled the reward delivery infusion syringe pump (PHM-107, Med Associates) and cage speaker (ENV-224AM, Med Associates) directly with the Med Associates cabinet.

Behavioral training

The training started with teaching the rats to maintain a steady hold on the lever. First, we acclimated the rats to the behavioral setup for one 30 min session. Then, we rewarded the rats with 3% sucrose water accompanied by a 12 kHz tone upon touching and/or moving the lever. After associating touching the lever with the reward, we used plexiglass walls to restrict the rats from using body parts other than the hand to press the lever. In gradual steps, we narrowed the gap between the restriction walls to 2 cm and automatically increased the holding duration in steps of 10 ms after each successful hold. If a rat used its mouth or both hands, we manually decreased the reward size, otherwise, we increased the reward size following successful trials. We inspected the preferred holding direction and hand of each rat. A hold was defined as moving and keeping the lever beyond a 1 mm threshold. Typically, the rats pulled the lever in the preferred horizontal direction to ∼5 mm until reaching a mechanical limit.

Next, we introduced the vibrotactile stimulus. To discourage timing, we randomized the holding duration until stimulus presentation between 600 and 1,600 ms with a 1:1 ratio (Figure 1A), and the allowed reaction time (RT) window was automatically decreased from 2,000 to 600 ms. The stimulus frequency was set to ∼200 Hz. Throughout the behavioral task, we used the 12 kHz tone clicker to indicate correct trials to the rats and white noise to indicate errors (premature/delayed releases). After an error, at least 1 s had to pass with the lever at the center until a new trial could begin (time-out).

Stereotaxic injections and implantation sites

The animals were initially anesthetized with isoflurane inhalation, followed by intraperitoneal injection of 75 mg/kg ketamine (Medistar, Holzwickede, Germany) and 50 mg/kg medetomidine (Orion Pharma, Espoo, Finland). The animals were put into a transportation container covered with an opaque cloth to facilitate the anesthetization. Once the animals were anesthetized, they were positioned in a stereotaxic frame (David Kopf Instruments, Tujunga, CA, USA), and their body temperature was maintained at 36°C–37°C using a rectal thermometer and a heated blanket (FHC, Bowdoin, USA). The animals were kept anesthetized using ∼1.0% isoflurane and 1.0 L/min O_2. For pre-surgery analgesia, we subcutaneously administered 0.05 mg/kg buprenorphine (Selectavet, Dr Otto Fischer GmbH, Weyarn/Holzolling, Germany). Every hour, we injected 2 mL of isotonic saline subcutaneously. We applied a moisturizing ointment to the eyes to prevent them from drying out (Bepanthen, Bayer HealthCare, Leverkusen, Germany). The skin was disinfected with Braunol (B. Braun Melsungen AG, Melsungen, Germany) and Kodan (Schülke, Norderstedt, Germany) using sterile cotton tips. A 2 cm-long incision of the skin on the head was opened using a scalpel. The exposed bone was cleaned using a 3% peroxide solution. Craniotomies were drilled bilaterally extending from −2 to +4.5 mm in the anterior-posterior direction and +1 to +4 mm in the mediolateral direction relative to bregma.

For photo-tagging experiments ($N = 3$ rats; Table S2), we injected 1 μL viral vector (rAAV5/hSyn-hChR2(H134R)-eYFP, UNC Vector Core, Chapel Hill, North Carolina) into the RFA. To inhibit RFA or CFA, we injected 1 μL of viral vector (rAAV5/hSyn-eNpHR3.0-eYFP, UNC Vector Core) into the respective region. For both photo-tagging and inhibition experiments we injected at two different depths (0.6 and 1.2 mm, 0.5 μL each).

For histological experiments three rats (Sprague-Dawley, female, 6–8 weeks of age) underwent bilateral stereotactic injections of AAV5/hSyn-eNpHR3.0-eYFP-WPREpA (UNC Vector Core, North Carolina, Chapel Hill, titer: 3.9x10 ^12) in RFA. Briefly, anesthesia was induced with 4% isoflurane (with O2 as the carrier gas), and rats were placed into a stereotactic apparatus (Stoelting, USA).

During the intervention, anesthesia was maintained between 1.5% and 2.0%. The surgical site was shaven, disinfected with Kodan (Schülke, Germany) and Braunol (B. Braun Melsungen AG, Germany) and topical anesthetic (2% xylocaine gel, Aspen Pharma Trading Limited, Ireland) applied over the incision site. The skin was incised by approx. 2cm, subcutaneous tissue removed and the craniotomies drilled using a fine drill. The injections were controlled by WPI micropump at a rate of 100 nL/min with a total volume of 350nL per site (see Table S4). To minimize the reflux of the injected volume, we left the injection needle in the tissue for 10 additional minutes before slowly extracting it from the brain. Post-operative care included subcutaneous injections of carprofen (5 mg/kg, every 24 h for up to 3 days) followed by weekly checks of weight and general wellbeing. Transcardiac perfusions were performed following 8 weeks of viral expression. On perfusion day, animals received an i.p. overdose of ketamine (100 mg/kg) and xylazine (10 mg/kg) with a maximum injection volume of 1 mL. For electron microscopy, rats were perfused with 0.05% glutaraldehyde (GA, science service 25% GA 1 mL Ampulle, item number E16220) and 4% PFA in 0.1 M phosphate buffer (PB). Brains were extracted and stored in fixative for 1 h and in PB overnight.

For experiments with inhibition of neurons projecting from RFA to CFA, we injected 1.4 μL of viral vector (rAAV2-retro.CAG-Cre, UNC Vector Core, North Carolina, Chapel Hill) at four different sites in both hemispheres of the CFA (two points separated by ∼0.5 mm in the anterior-posterior axes at depths of 0.6 and 1.2 mm, 0.35 μL at each point). We injected two sites in the RFA with 0.75 μL of viral vector in both hemispheres (rAAV5/EF1a-DIO-eNpHR3.0-eYFP, UNC Vector Core) at depths of 0.6 and 1.2 mm (0.35 μL at each location; Table S3). We injected the respective areas at a rate of 100 nL/min using a 10 μL gas-tight Hamilton syringe (World Precision Instruments, Sarasota, Florida). To minimize reflux of the injected volume, we left the injection needle in the tissue for 10 additional minutes before slowly extracting it from the brain.

For electrophysiological recordings, we inserted 2-shank, 32-channel laminar probes (E32+R-150-S2-L6-200-NT, ATLAS Neuroengineering, Leuven, Belgium) into the contralateral hemisphere relative to the forepaw used in the experiment (N = 5 rats each with probes in the RFA or CFA, N = 10 rats overall; Table S1). The probe was slowly inserted into the brain while the rat was held with a vacuum holder (ATLAS Neuroengineering, Leuven, Belgium).

We applied a sealant (Kwik-Cast, World Precision Instruments) over the craniotomy and fixed the probe and/or optical fibers to the skull with UV-cured dental cement (RelyX, 3M, Saint Paul, MN). Self-tapping skull screws (J.I. Morris Company, Southbridge, Massachusetts) acting as a reference for extracellular recordings were placed above the cerebellum. For increased stability and reduced noise, we also cemented the custom-made electrode interface board. Rats were given >7 days of recovery before further experiments.

Data acquisition

We performed electrophysiological recordings during 3–4 sessions per rat with at least one week break in between sessions (minimum 15 correct trials). To avoid electrical artifacts, we built another behavioral setup inside a Faraday cage and disconnected the touch sensor. We sampled the broadband signal at ∼25 kHz using a digital head stage (ZD32, Tucker-Davis Technologies (TDT), Alachua, Florida). Spiking activity was bandpass filtered between 300 and 5,000 Hz. The Med Associates system registered behavior at 100 Hz and synchronized with the electrophysiological signal via TTL communication.

Photo-tagging experiments were conducted eight weeks after the viral injection. Laser stimulation was conducted at 473 nm with a power of 1, 2, 4 or 8 mW out of a 200 μm optical fiber with at least 30 trials for each power setting at the end of the behavioral sessions during continued neuronal recordings (N = 3 rats, 1 session per rat).

For the photoinhibition experiments, we inhibited the CFA or RFA during either the preparation or movement periods. We used light with a wavelength of 590 nm at 15–20 mW for 0.5 s or until movement initiation (50% of trials). After the behavioral session, we inhibited for 0.5 s with an inter-stimulus period of 10 s to characterize responses outside the task context.

QUANTIFICATION AND STATISTICAL ANALYSIS

Behavior

Reaction times (RTs) were computed from the stimulus onset until the rat released the lever. Lever release was defined as the movement of the lever laterally to an amplitude of at least 2 mm. For analysis of optogenetic effects and all electrophysiological analyses, trials with release times less than 100 ms after the cue were discarded to avoid ambiguities if a release should be considered spontaneous or cued. For comparing behavioral performance in optogenetics experiments across regions, we performed bootstrapping (n = 1000) by drawing 15 sessions with replacement and calculating the mean premature release rate (PR) across sessions. We then present the median and CI of these bootstrap samples for each region.

Electropysiology

We sorted the broadband signal into units using KiloSort,[89] inspected each cluster, and defined units based on wave shape. The binary spike-time array (1 for spike, 0 otherwise) of each unit was smoothed into firing rate (FR) with a Gaussian kernel with a standard deviation of 50 ms and then normalized (Z score).

Cell classification

To identify task-modulated units, neuronal activity was aligned to movement onset. Activity within a 1-s window immediately preceding movement onset (pre-movement phase) was compared to activity within a 1-s window following movement onset (movement

phase). Statistical significance was assessed using a *t* test with a threshold of $p < 0.05$. Modulated units from RFA and CFA were then pooled and classified using k-means unsupervised clustering. The optimal number of clusters was determined using silhouette analysis.

Photo-tagging

In photo-tagging experiments, a neuron was considered as 'tagged' if it fulfilled three criteria: (1) a light pulse of 1 ms caused an action potential in the recorded single unit for at least 60% of the laser pulses; (2) the light-induced action potential waveform was similar to the mean of the spontaneously occurring waveforms with a Pearson correlation coefficient higher than 0.7, and (3) the induced action potential occurred within a latency window of 15 ms, which was in line with the timing of antidromically-evoked action potentials[91] (Figure 3D). We further performed a post-hoc collision test on the putatively tagged units (Figure S3). In 10 of the 23 putatively tagged units, we were unable to initiate an antidromic action potential when the neuron exhibited spontaneous action potential within 10 ms prior to the laser pulse. We then characterized the latency and jitter of all putatively tagged neurons, finding no differences between those that passed the collision test and those that could not be tested due to inactivity before the laser pulse. Consequently, we grouped all neurons together as projecting from the RFA to the CFA.

Modulation by RFA silencing

To determine if a CFA neuron is modulated by inhibition from neurons projecting from the RFA to the CFA, we compared the FR of the neuron during the pre-movement and movement periods, with and without laser inhibition. A *p*-value of less than 0.05 indicated that the neuron was significantly modulated by the inhibition.

Principal component analysis

PCA was performed using the jPCA toolbox[90] without subtracting the cross-condition mean. The raw PCA output was used for all further analysis. The preparation, or null space was defined in the first PCA plane by the vector from −1.2s prior to cue to the cue onset. The movement-potent direction was defined as being orthogonal to the preparation direction. To analyze deviations from control, we calculated the differences between the manipulations and control for the movement-null and potent directions and z-scored these differences by the mean and standard deviation in the pre-laser period.

Histology

For the histological verification of eNpHR3.0, we killed the animals by administering 400 mg/kg sodium pentobarbital (Release500, WDT, Garbsen, Germany) and transcardial perfusion with PBS followed by ice-cold 4% paraformaldehyde. After removing the brains, we post-fixed the tissue for 2 additional days before transferring it into a solution of 30% w/v sucrose (Merck KGaA, Darmstadt, Germany) in water at 4°C for equilibration. Brains transferred from a sucrose solution were attached to the cooling block of a microtome with Tissue Tek (Sakura Finetek, Fisher Scientific, Germany) and were sectioned into 50 μm thin slices. The slices were transferred to phosphate-buffered saline (PBS) with 0.01% sodium azide. For antibody staining, selected slices were washed for 3 × 10 min in PBS on a rotary shaker at room temperature. The slices were blocked and permeabilized for 1 h (PBS 0.01 M/Triton 0.4%/BSA 5%, Sigma Aldrich, St. Louis, MO, USA) on the rotary shaker. The first antibody (dilution 1:1,000, monoclonal anti-Parvalbumin, P3088, Merck, Taufkirchen, Germany) was applied overnight at 4°C (PBS 0.01 M/Triton 0.2%). The slices were washed for 3 × 10 min in PBS on the rotary shaker at room temperature. The second antibody (dilution 1:250, Cy3 goat anti-mouse, M30010, Thermofisher, Waltham, MA, USA) was applied for 3 h (PBS 0.01 M/Triton 0.2%). Finally, the slices were washed for 3 × 10 min in PBS on the rotary shaker at room temperature and mounted. The slices were imaged with a Zeiss (Oberkochen, Germany) LSM880 confocal microscope using a 40× objective.

Electron microscopy

Brains were sectioned with a vibratome into 50 μm slices and washed in 50 mM TBS (6 g TRIS, 9 g NaCl in 1 L aqua bidest, pH 7.6) for 1 h. Slices were blocked in 20% NGS in TBS for 1 h and incubated overnight with primary antibodies (rabbit anti-GFP and mouse anti-PV; 1:100) in TBS +2% NGS at 4°C. After incubation, slices were washed in TBS for 1 h. Secondary antibodies were then applied overnight (Nanogold 1.4 nm goat anti-rabbit, and biotinylated goat anti-mouse; 1:100 in TBS +2% NGS). On the next day, slices were washed for 30 min in TBS, postfixed for 10 min in 1% GA in 25 mM PBS, washed for 15 min in 25 mM PBS, and briefly rinsed (2 × 30 s) in distilled water. For silver intensification of Nanogold-labeled EYFP-positive presynaptic terminals, HQ-Silver (Nanoprobe; 2 drops A, B, C) was applied at 15°C for 5 min, followed by a 1 h wash in 50 mM TB. For visualization of PV-positive structures, slices were processed using the ABC method (4410 μL TB, 1 drop A, 1 drop B) for 90 min at room temperature, washed for 30 min in 50 mM TB, and developed with DAB (Sigma Fast) for 3.5 min. Slices were then washed (30 min in 50 mM TB and 10 min 0.1 PB), postfixed in 0.5% OsO_4 with 6.8% sucrose for 40 min, dehydrated through graded ethanol solutions, contrasted with 1% uranyl acetate in 70% ethanol, and embedded in Durcupan. Ultrathin sections (60 nm) were cut with a Leica UC 6 ultramicrotome, stained with lead citrate (Reynolds), and imaged using a LEO 906 transmission electron microscope (Zeiss) equipped with a SharpEye 2k CCD camera. Images were processed using ImageSP (Tröndle, Germany). Synaptic contacts exhibiting thick postsynaptic density (asymmetric) were classified as putative glutamatergic excitatory synapses, whereas synaptic contact with thin postsynaptic density (symmetric) were classified as putative GABAergic inhibitory synapses.

Statistical tests

Data are represented as mean ± SEM or 95% confidence intervals (CI). All statistical analyses were computed in MATLAB (Mathworks, version R2018b and R2024a).

Decoding lever position from neural activities

We used a linear regression model to decode the lever position from the neural activities. For each trial, the input features were the firing rates of all neurons from the trial initiation to the lever release, binned into 200 ms intervals. The output is the mean lever position in the corresponding 200 ms interval. The model was trained independently for each session, and the R^2 score was used to evaluate the decoding performance. For each model, we formulated a baseline model by shuffling the neural activities across trials, and the R^2 score of the baseline model was subtracted from that of the original model to obtain the adjusted R^2 score. R^2 scores are presented as mean ± SEM.

Inverse reinforcement learning

MDP formulation

We modeled the preparation-movement task as a Markov decision process (MDP). Intuitively, this MDP models the preparation-movement task as a sequence of decision steps in 0.2s bins: at each step, the animal decides whether to hold or release the lever, with the task resulting in either success or error as an outcome. Formally, it is denoted by a five-tuple (S, A, P, r, γ), where S and A denote the set of states and actions, respectively.

The function P: $S \times A \times S \to [0, 1]$ is the state transition function. The function r: $S \times A \to \mathbf{R}$ defines the reward function, and $\gamma \in [0, 1]$ denotes the discount factor. Additionally, the function π: $S \times A \to [0, 1]$ is used to represent the policy according to which actions are selected in the MDP. To formulate the MDP for the preparation-movement task, the set of states S was defined by discretizing the time into chunks of 0.2 s, plus two auxiliary states (success and failure), i.e., S = {0.0 s, 0.2 s, …, 2.4 s} ∪ {success, failure}. In every state, the agent could pick an action from the set of actions A = {stay, release}. We defined the MDP to have deterministic transitions. The discount factor was set to 1 in all experiments, i.e., no discount. The reward function r was considered to be unknown and to be learned from animal behavior.

This MDP formulation builds the basis for the estimation of intrinsic immediate reward. For this, we apply an inverse reinforcement learning method to learn the unknown reward function r. Intuitively, we assume the animal to act quasi-optimally with respect to what it believes to yield the best long-term outcome. This assumption allows us to pinpoint recorded behavior to the underlying immediate reward: since frequently chosen actions must reflect high expected long-term value, the observed action frequencies at each state sufficiently constrain the reward to be recovered in closed form. Once found, we can then reconstruct the immediate reward function from a parameterized combination of neuronal activities, which in turn allows for modulation of these neuronal activities to simulate new behavior.

Estimation of intrinsic reward

Formally, the estimation of intrinsic reward can be formulated as the following optimization problem: We apply an inverse reinforcement learning method to learn the unknown reward function r, which can be formulated as the following optimization problem:

$$\begin{aligned} &\text{maximize } \mathbf{E}_{\xi\sim D}[\log \mathbf{P}(\xi \mid \pi_r)] \\ &\text{subject to } \pi_r(s,a) = \exp\Big(Q(s,a) - \log \sum \exp Q(s,\cdot)\Big), \text{for all } s \in \mathcal{S}, a \in \mathcal{A} \\ &Q(s,a) = r(s,a) + \gamma \sum_{s' \in S} P(s,a,s') \max_{a' \in \mathcal{A}} Q(s',a'), \text{for all } s \in \mathcal{S}, a \in \mathcal{A}, \end{aligned} \qquad \text{(Equation 1)}$$

where r is the optimization variable and D, the set of animal demonstrations, is the problem data. The set D consists of multiple trajectories represented as a sequence of state-action pairs: $\xi = \{(s_0, a_0), \ldots, (s_n, a_n)\}$. The objective of problem (Equation 1) is maximized when the animal policy $\pi^E(s, a)$ is equivalent to $\pi_r(s, a)$. Assuming that the actions taken by the animal are samples from a Boltzmann distribution over its optimal action values, we have

$$\pi^E(s,a) = \frac{\exp(Q(s,a))}{\sum_{a' \in \mathcal{A}} \exp(Q(s,a'))} \implies Q(s,a) = Q(s,b) + \log\big(\pi^E(s,a)\big) - \log\big(\pi^E(s,b)\big), \qquad \text{(Equation 2)}$$

for all actions $a \in A$ and $b \in A_{-a}$ where $A_{-a} = A \backslash \{a\}$. Using the Bellman optimality equation in Equation 2, the immediate reward of action a in state s can be expressed by the immediate reward of some other action $b \in A_{-a}$, the respective log-probabilities and future action-values[90]:

$$r(s,a) = \mu(s,a) + \frac{1}{|\mathcal{A}_{-a}|} \sum_{b \in \mathcal{A}_{-a}} (r(s,b) - \mu(s,b)), \qquad \text{(Equation 3)}$$

where $|A_{-a}|$ denotes the cardinality of A_{-a}, and

$$\mu(s,a) = \log\big(\pi^E(s,a)\big) - \gamma \sum_{s' \in S} P(s,a,s') \max_{a' \in \mathcal{A}} Q(s',a'). \qquad \text{(Equation 4)}$$

Let $|A| = m$, for each state $s \in S$, formulating Equation 3 for all actions $a \in A$ results in a system of linear equations about $r(s, \cdot)$:

$$\begin{bmatrix} 1 & -\frac{1}{m-1} & \cdots & -\frac{1}{m-1} \\ -\frac{1}{m-1} & 1 & \cdots & -\frac{1}{m-1} \\ \vdots & \vdots & \ddots & \vdots \\ -\frac{1}{m-1} & -\frac{1}{m-1} & \cdots & 1 \end{bmatrix} \begin{bmatrix} r(s,a_1) \\ r(s,a_2) \\ \vdots \\ r(s,a_m) \end{bmatrix} = \begin{bmatrix} \mu(s,a_1) - \frac{1}{m-1}\sum_{b \in \mathcal{A}_{-a_1}} \mu(s,b) \\ \mu(s,a_2) - \frac{1}{m-1}\sum_{b \in \mathcal{A}_{-a_2}} \mu(s,b) \\ \vdots \\ \mu(s,a_m) - \frac{1}{m-1}\sum_{b \in \mathcal{A}_{-a_m}} \mu(s,b) \end{bmatrix}. \quad \text{(Equation 5)}$$

Thus the unknown reward function r can be obtained by solving Equation 5 for all $s \in S$ via least squares.

Mapping neuronal activities to intrinsic reward

We assume the intrinsic reward function can be approximated as

$$r(s,a) \approx \widehat{r}(\Psi(s),a) = f_\theta(\Psi(s),a), \quad \text{(Equation 6)}$$

where $\Psi(s) \in \mathbf{R}^n$ is the feature vector obtained from the average activities of n neurons under state s, and $f_\theta : \mathbf{R}^n \times \mathcal{A} \to \mathbf{R}$ is some function parameterized by θ (e.g., a linear transformation or a neural network).

The parameters θ are fitted to represent intrinsic reward $r(s, a)$ and hence the underlying behavior of the recorded animals as closely as possible. Specifically, the parameters θ can be obtained via either least squares or gradient descent, depending on the class of the function f_θ, according to the distance between $r(s, a)$ and

$\widehat{r}(\Psi(s), a)$ measured by $\|r(s,a) - \widehat{r}(\widetilde{\Psi}(s),a)\|_2^2$. Then the fitted parameters can contribute to generalization to any arbitrary neuronal activities $\widetilde{\Psi}(s)$ obtained, e.g., from perturbation of recorded activities. The procedure of NeuRL was applied to individual trials of the whole dataset of one session.

Behavior decoding from neuronal activities

We decode the animal behavior from neuronal activities according to the approximated intrinsic reward $\widehat{r}(\Psi(s), a)$ from Equation 6. For this purpose, we take a function f_θ from the class of neural networks. After fitting the parameters θ of the map f_θ, the optimal action-value function can be approximated similarly by solving the Bellman optimality condition

$$\widehat{Q}(\Psi(s),a) = \widehat{r}(\Psi(s),a) + \gamma \sum_{s' \in S} P(s,a,s') \max_{a' \in \mathcal{A}} \widehat{Q}(\Psi(s'),a') \quad \text{(Equation 7)}$$

for all $s \in S$ and $a \in A$. Then the predicted animal policy can be expressed as

$$\widehat{\pi}(\Psi(s),a) = \frac{\exp(\widehat{Q}(\Psi(s),a))}{\sum_{a' \in \mathcal{A}} \exp(\widehat{Q}(\Psi(s),a'))}. \quad \text{(Equation 8)}$$

This process is performed individually for each recorded trial.

Simulated inhibition of neuronal activities

We simulate the optogenetic inhibition of animal brain activities according to the following procedure. In this specific experiment we take the feature vector $\Psi(s)$ by averaging over all trials for each animal, and consider the function f_θ to be a linear transformation. First to find the parameters θ of the map f_θ, we solve the following least squares problem with Tikhonov regularization:

$$\text{minimize} \quad \|f_\theta(\Psi(s),a) - r(s,a)\|_2^2 + \lambda\|\theta\|_2^2, \quad \text{(Equation 9)}$$

where θ is the variable and the hyperparameter λ controls the "size" of θ, which can be considered as the strength of the following inhibition process. Analogous to real-world inhibition experiments, we then manipulate the feature vector $\Psi(s)$ by setting the feature from targeted neurons within the targeted response window to zero to obtain the perturbed feature vector $\widetilde{\Psi}(s)$ for all $s \in S$. Finally we use the fitted parameters θ from Equation 9 to get the perturbed reward function $\widetilde{r}(\Psi(s), a)$, and the same process described in Equations 7 and 8 is applied to obtain the simulated animal policy under inhibition. In the results shown in Figure S3, the hyperparameter $\lambda = 0.2$.

Cell Reports, Volume *45*

Supplemental information

Mechanisms of premotor-motor cortex interactions during movement initiation

Mansour Alyahyay, Julian J. Ammer, Gabriel Kalweit, Hao Zhu, Ahmed Adzemovic, Maria Kalweit, Golan Karvat, Artur Schneider, Yixin Tong, Mate D. Döbrössy, Zoe Jäckel, Cemal Akmese, Andreas Vlachos, Joschka Boedecker, and Ilka Diester

Supplemental Information

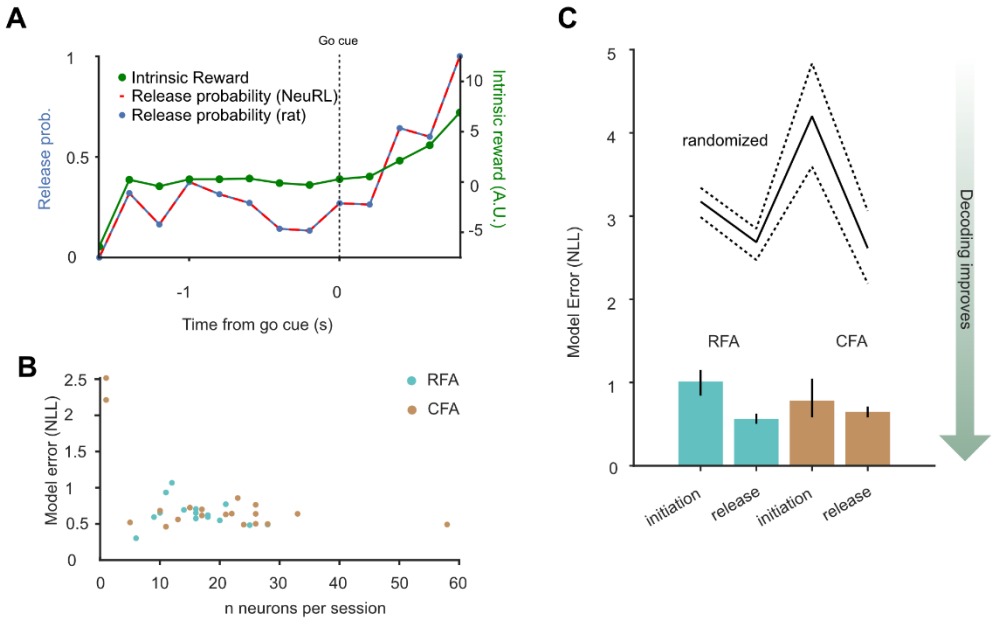

Figure S1. NeuRL decoding, related to Figure1.

(A) Learned intrinsic reward (green) and the resulting performance as probability of release for each time bin (red dashed line) plotted with the actual release probability of one example rat (blue).

(B) Model error for the decoding of lever release with NeuRL in RFA and CFA (N = 5 rats) for all sessions as a function of number of neurons per session.

(C) Decoding of task initiation and lever release with NeuRL in RFA and CFA (N = 5 rats). The model error for decoding the release time via NeuRL was quantified as negative log likelihood (NLL). Error bars depict 95% confidence intervals.

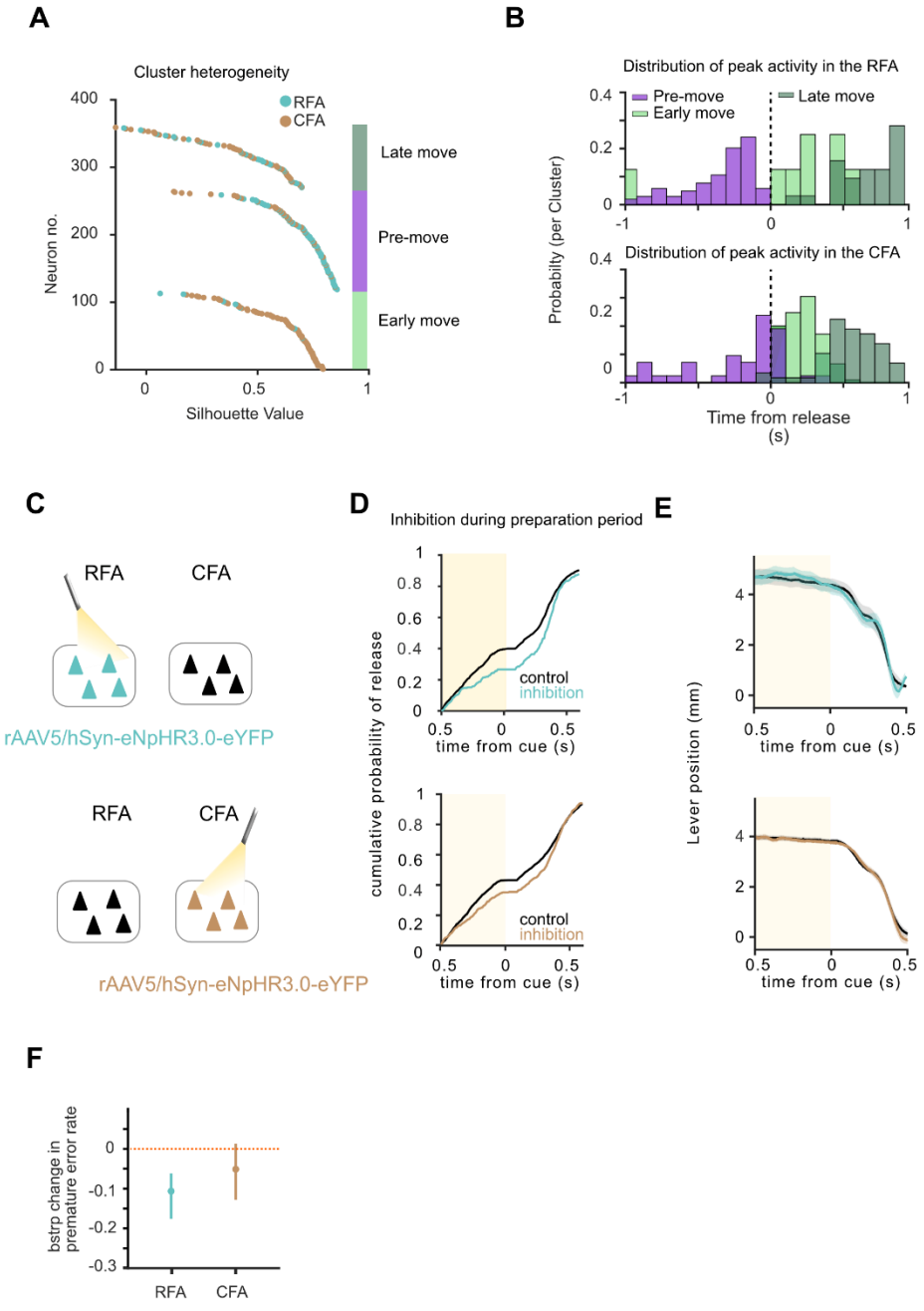

Figure S2. Cluster heterogeneity and effect of individual optogenetic inhibition of RFA or CFA, related to Figure 2.

(A) Silhouette plots illustrating the heterogeneity in the k-means clusters. Closed circles, individual units.

(B) Probability distribution of peak activity times normalized for each cluster for RFA (top) and CFA (bottom). Note that despite the heterogeneity within clusters, neurons are split into clusters with predominantly pre-movement, early movement and late movement neurons.

(C) Top: Schematic of optogenetic manipulation in RFA, rAAV5/hSyn-eNpHR3.0-eYFP was injected into RFA and a fiber implanted. Bottom: Optogenetic manipulation in CFA.

(D) Top: Average cumulative release time (N = 3 rats, n = 15 sessions) in response to 0.5 s inhibition in RFA prior to the cue in blue. Control condition in black. Bottom: Inhibition in CFA (N = 4 rats, n = 23 sessions) in brown.
(E) Top: Average lever trajectories in correct trials (N = 3 rats, n = 15 sessions) in response to 0.5 s inhibition in RFA prior to the cue in blue. Control condition in black. Bottom: Inhibition in CFA (N = 4 rats, n = 23 sessions) in brown. Note that there is no effect of optogenetic inhibition on lever position during the preparation phase.
(F) Median bootstrapped change in premature error rate with 95% confidence interval for RFA (blue) and CFA (brown), dashed line indicates 0 change, n = 1000 bootstraps with mean of n = 15 sessions each.

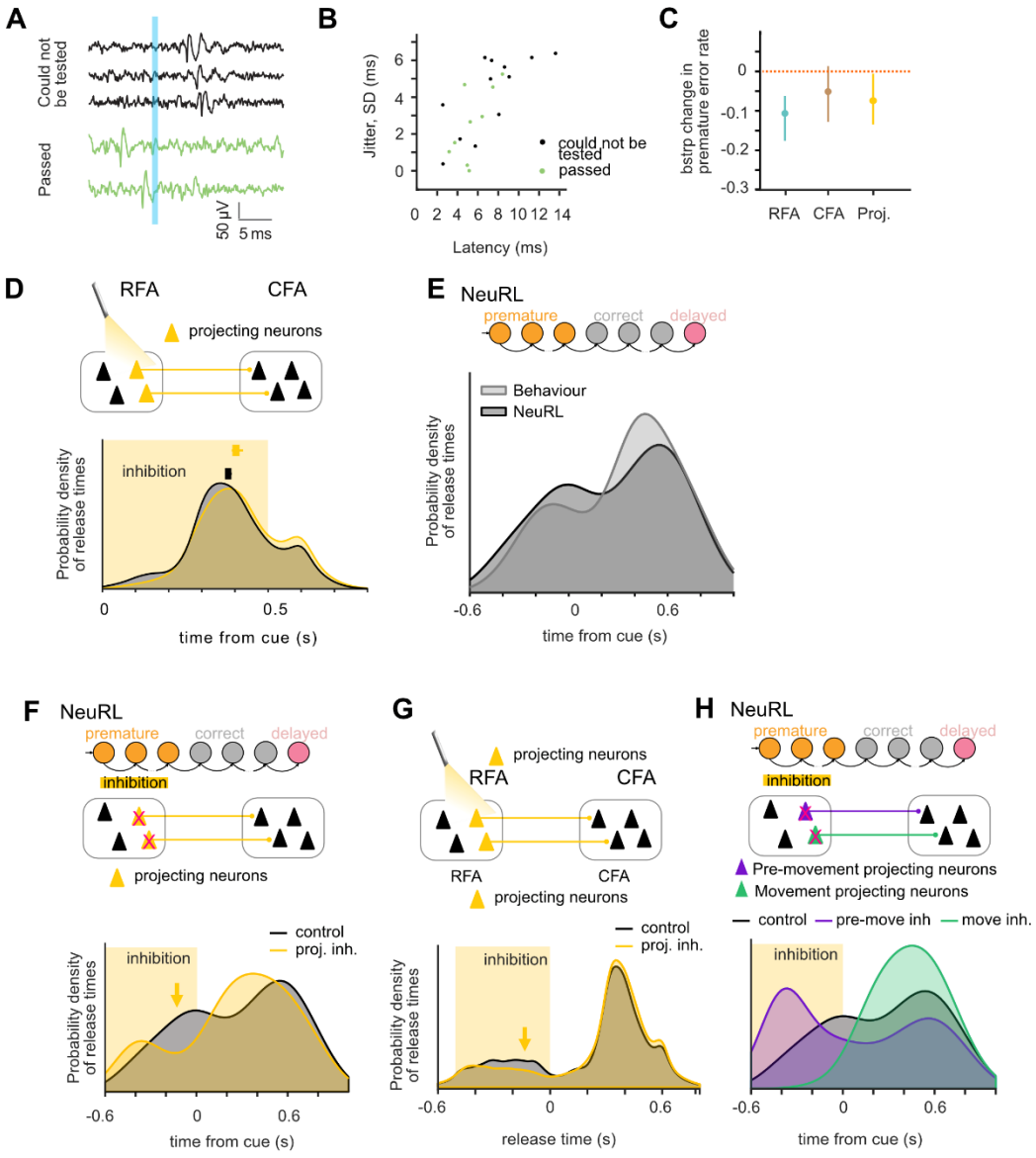

Figure S3. Spontaneous collision test and behavioral predictions by NeuRL, related to Figure 3.
(A) Example traces for photo-triggered spikes without (black) and with (green) preceding spontaneous action potential.
(B) Scatter plot of spike timing jitter and spike latency of first spike after laser onset. Green dots refer to units that passed the collision test, i.e. a spontaneously occurring spike before the optogenetic stimulation pulse prevented the backpropagation or generation of an antidromic spike. Black dots refer to units which could not be tested due to the absence of spontaneously occurring spikes preceding the laser pulse.
(C) Median bootstrapped change in premature error rate with 95% confidence interval for RFA (blue), CFA (brown) and RFA to CFA projecting neurons (yellow) dashed line indicates 0 change, n = 1000 bootstraps with mean of n = 15 sessions each. Data are replotted from Fig S2G and Fig 3I.
(D) Top: Schematics for inhibition of neurons projecting from RFA to CFA. Bottom: Probability density of release times in control (black) and after inhibition (yellow) during the movement period relative to cue onset (N = 4 rats with n = 32 sessions).

(E) Probability density of release times in control behaviour (black, N=3 rats), and for the NeuRL model (gray). Behavioural data was binned in 200ms bins for a direct comparison with NeuRL.
(F) Top: Schematics for *in silico* inhibition of putative RFA to CFA projecting neurons. We inhibited RFA to CFA-projecting neurons during the pre-movement period (N = 3 rats, 1,000 simulations for each rat), using NeuRL. Bottom: Probability density of release times for control (black) and inhibition of projecting neurons (yellow). Note that NeuRL was trained on neural activity recorded in a first cohort subjected to electrophysiology only, whereas optogenetic experiments were performed in a second cohort without electrophysiological recording (Fig 3 H). Note, that the model also predicts a leftward shift in the peak of the release time distribution following the cue which we did not observe in the optogenetic experiments in E.
(G) Top: Schematics for inhibition of neurons projecting from RFA to CFA. Bottom: Probability density of release times in control (black) and after inhibition (yellow) during the preparation period (N = 4 rats with n = 32 sessions).
(H) Schematics for *in silico* inhibition of subpopulations of putative RFA to CFA projecting neurons. Probability density of release times in control (black), and when inhibiting the pre-movement subpopulation (purple) or movement subpopulation (green) during the preparation period.

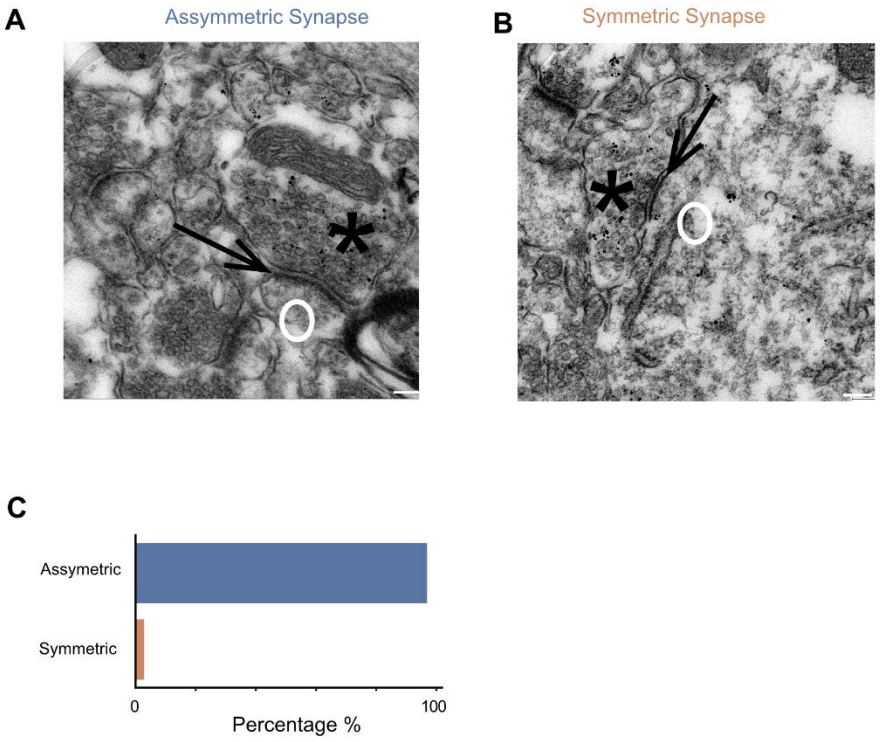

Figure S4. Asymmetry of synapses, related to Figure 4.
(A) EM image showing an asymmetric synapse. Asterisk: presynapse, circle: post synapse, arrow: synaptic cleft. Note the thick post synaptic density.
(B) Same as A for symmetric synapse.
(C) Percentage of asymmetric and symmetric synapses.

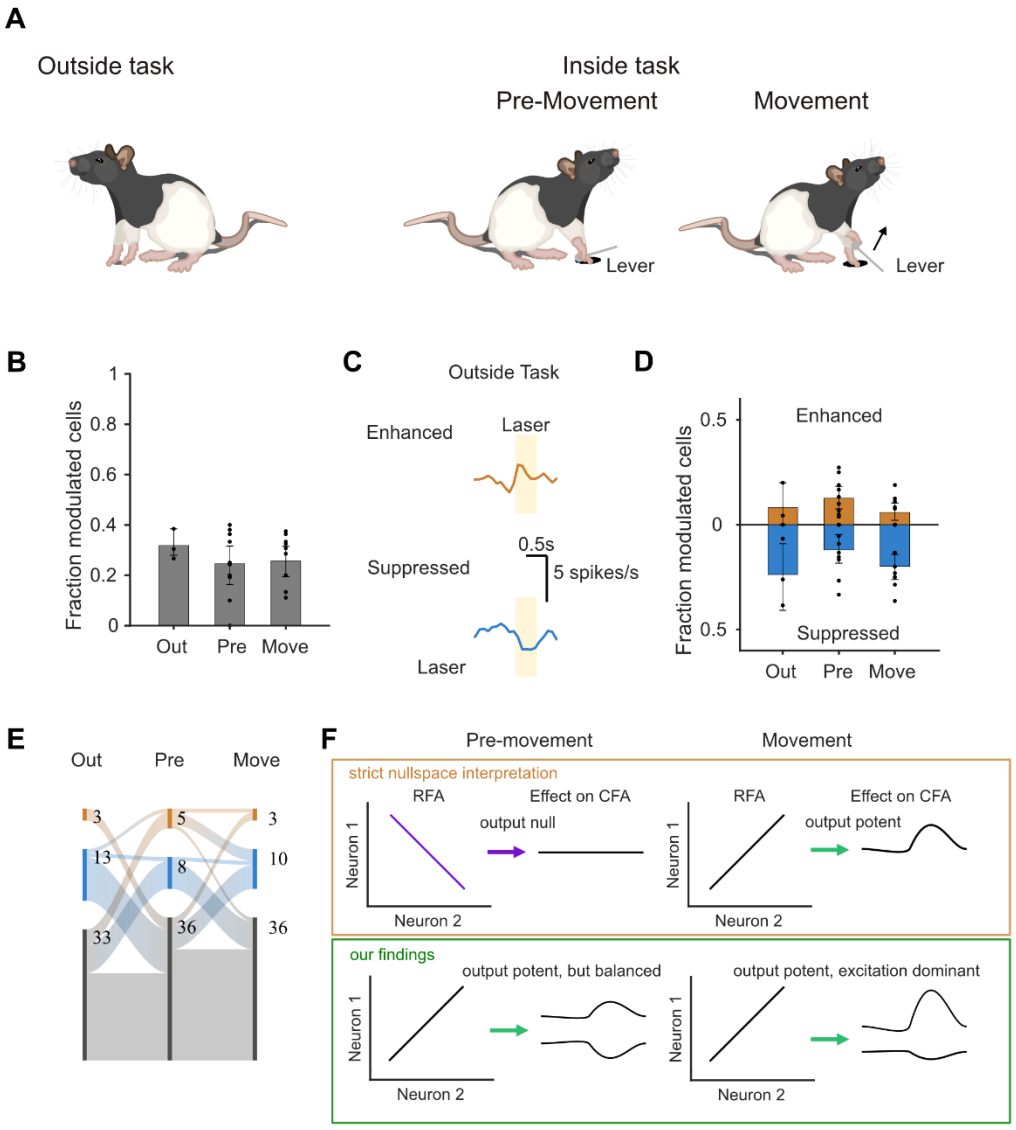

Figure S5. CFA responses to RFA input modulation outside the task, during pre-movement and during movement, related to Figure 5.

(A) Schematic of the investigated behavioral epochs. Optogenetic experiments were performed either outside the task, during the preparation period, or the movement period.

(B) Fractions of modulated cells, single dots refer to individual sessions. Error bars depict 95% confidence intervals.

(C) Average of enhanced and suppressed neuron populations when silencing RFA outside the task.

(D) Fraction of enhanced and suppressed cells across task states. Error bars depict 95% confidence intervals.

(E) Sankey plot illustrating the reorganization of CFA neurons influenced by RFA input. Distinct populations are affected outside the task and during preparation.

(F) Simplified schematic of possible communication schemes between RFA and CFA during pre-movement (left) and movement (right). Please note that output potent does not necessarily mean movement potent.

Rat #	Recording area	Injection coordinates		
		AP (mm)	ML (mm)	DV of shank tip (mm)
10	RFA	+3.8	-1.7	2.4
12	RFA	+3.7	-1.5	2.4
504	RFA	+3.2	-1.9	2.4
533	RFA	+3.5	-2.0	2.4
546	RFA	+3.5	-2.0	2.4
1	CFA	+0.2	-2.2	2.4
3	CFA	+0.6	-2.5	2.4
13	CFA	-0.1	-2.1	2.4
16	CFA	+0.3	-2.8	2.4
506	CFA	-0.5	-2.4	2.4

Table S1: Coordinates of silicon probe implantation sites in the RFA and CFA. Related to Figure 1.

Rat #	Injection area	Viral vector	Injection coordinates			Laser area	Recording area
			AP (mm)	ML (mm)	DV of shank tip (mm)		
10	RFA	AAV-hSyn-ChR2	+3.5	-1.5	2.4	CFA	RFA
12	RFA	AAV-hSyn-ChR2	+3.4	-1.6	2.4	CFA	RFA
546	RFA	AAV-hSyn-ChR2	+3.5	-1.5	2.4	CFA	RFA

Table S2: Injection coordinates in photo-tagging experiments. Related to Figure 3.

Rat #	Injection area	Viral vector	Coordinates left (mm)			coordinates right (mm)			Laser area	Recording area
			AP	ML	DV	AP	ML	DV		
3	RFA	AAV-DIO-eNpHr	3.7	1.5	0.6/1.2	3.6	1.7	0.6/1.2	RFA	CFA
	CFA	retroAAV-cre	0.5/0.0	2.2/2.3	0.6/1.2	0.7/0.1	2.5/2.5	0.6/1.2		
13	RFA	AAV-DIO-eNpHr	3.8	3.5	0.6/1.2	3.5	1.5	0.6/1.2	RFA	CFA
	CFA	retroAAV-cre	0.37/0.4	0.5/0.0	0.6/1.2	0.50/0.0	2.4/2.3	0.6/1.2		
15	RFA	AAV-DIO-eNpHr	3.3	3.4	0.6/1.2	3.4	1.4	0.6/1.2	RFA	N/A
	CFA	retroAAV-cre	0.2/-0.4	0.7-0.1	0.6/1.2	0.7/-.1	2.8/2.6	0.6/1.2		
16	RFA	AAV-DIO-eNpHr	3.4	3.6	0.6/1.2	3.6	1.6	0.6/1.2	RFA	CFA
	CFA	retroAAV-cre	0.4/-0.2	1.0/0.6	2.2/2.3	1.0/0.6	2.62.5	0.6/1.2		

Table S3: Injection coordinates, silicon probes, and optical fiber implantation location for inhibition experiments. Related to Figure 5.

Rat #	Injection area	Injection coordinates		
		AP (mm_)	ML (mm)	DV (mm)
19	RFA	+3.5	+/- 1.5	-1.2, -0.6
4	RFA	+3.5	+/- 1.5	-1.2, -0.6
5	RFA	+3.5	+/- 1.5	-1.2, -0.6
8	RFA	+3.5	+/- 1.5	-1.2, -0.6

Table S4: Injection coordinates for EM experiments. Related to Figure 4.